Nanoscale

RSC Publishing

REVIEW

View Article Online
View Journal | View Issue

Cite this: *Nanoscale*, 2013, **5**, 4015

Focusing on luminescent graphene quantum dots: current status and future perspectives

Lingling Li,† Gehui Wu,† Guohai Yang, Juan Peng, Jianwei Zhao* and Jun-Jie Zhu*

Received 27th November 2012
Accepted 7th January 2013

DOI: 10.1039/c3nr33849e

www.rsc.org/nanoscale

To obtain graphene-based fluorescent materials, one of the effective approaches is to convert one-dimensional (1D) graphene to 0D graphene quantum dots (GQDs), yielding an emerging nanolight with extraordinary properties due to their remarkable quantum confinement and edge effects. In this review, the state-of-the-art knowledge of GQDs is presented. The synthetic methods were summarized, with emphasis on the top-down routes which possess the advantages of abundant raw materials, large scale production and simple operation. Optical properties of GQDs are also systematically discussed ranging from the mechanism, the influencing factors to the optical tunability. The current applications are also reviewed, followed by an outlook on their future and potential development, involving the effective synthetic methods, systematic photoluminescent mechanism, bandgap engineering, in addition to the potential applications in bioimaging, sensors, *etc.*

1 Introduction

Carbon, one of the most abundant elements on the earth, brings us star materials over and over again. The football-shaped fullerenes, discovered in 1985 by Smalley *et al.*[1] and the needle-liked carbon nanotubes (CNTs), first characterized in 1991 by Iijima,[2] both as new allotropes of carbon, attract great interests from scientists of chemistry, physics, biology and medical science. Graphitic forms include 0D fullerene, 1D CNT and 3D graphite, and the 2D case comes to the graphene, a single layer of carbon atoms formed in honeycomb lattice, which was rewarded with the 2010 Nobel Prize in Physics. Since the discovering in 2004 by Geim and Novoselov *et al.* using sticky tape to peel atomically thin layers of graphene from lumps of graphite,[3] graphene meets an explosion of research for its exceptional thermal, mechanical and electronic properties.[4] As graphene is a zero-bandgap material, the possibility for the observation of its luminescence is almost impossible, which impedes its application in optoelectronics.[5,6] Nevertheless, graphene exhibits an infinite exciton Bohr radius, thus quantum confinement could take effect in graphenes of any finite size and is expected to result in many interesting phenomena that cannot be obtained in other semiconductors.[7] In principle, the bandgap of graphene can be tuned from 0 eV to that of benzene by varying their sizes.[8] Consequently, graphene quantum dots (GQDs), as a new kind of quantum dots, have emerged and ignited tremendous research interest. Due to the pronounced quantum confinement and edge effects, GQDs

State Key Laboratory of Analytical Chemistry for Life Science, School of Chemistry and Chemical Engineering, Nanjing University, Nanjing, 210093, P. R. China. E-mail: jjzhu@nju.edu.cn; zhaojw@nju.edu.cn

† These authors contributed equally to this work.

Lingling Li received her PhD degree with Prof. Jun-Jie Zhu and Prof. Jian-Rong Zhang in chemistry from the School of Chemistry and Chemical Engineering, Nanjing University in 2011. Currently, she is a post-doctoral researcher at Nanjing University. Her research interests focus on preparation of novel quantum dots and their applications in electrochemiluminescence studies.

Gehui Wu received his BS degree from Xiamen University in China in 2011. He is currently a master student with Professor Jun-Jie Zhu and Professor Jianwei Zhao at Nanjing University, China. His research involves graphene quantum dots and multifunctional nanocomposites.

assume numerous novel chemical/physical properties.[9,10] Besides, GQDs also show low cytotoxicity, excellent solubility, chemical inertia, stable photoluminescence, better surface grafting, thus making them promising in optoelectronic devices, sensors, bioimaging, *etc.*[9–18] In addition to convert 1D graphene to 0D GQDs, the surface chemistry-tuned methods, such as varying the oxidation of graphene, modification of graphene oxide (GO), reduced GO (r-GO) and doping r-GO, as well as the production of 1D graphene nanoribbons, can also bring about fluorescent graphene-based nanomaterials.[19–27] Besides, fluorescent carbon nanotubes (CNTs) have also been reported.[28–30] However, the large size of graphene and CNTs limits their direct application in nanodevices.

Another two examples of 0D carbon-based fluorescent nanomaterials, diamond nanocrystals (DNs)[31,32] and carbon dots (CDs)[33,34] have also attracted much attention in recent years. Special attention should be paid to distinguish these three types of nanomaterials. In general, DNs consist of about 98% carbon with residual hydrogen, oxygen, and nitrogen, possess a sp^3 hybridized core, and have small amounts of graphitic carbon on the surface. DNs emit from point defects, particularly the negatively charged nitrogen vacancy site.[35] The CDs are usually prepared by laser ablation or electrochemical oxidation of graphite,[36–38] electrochemical soaking of carbon nanotubes,[39] thermal oxidation of suitable molecular precursors, *etc.*[40–43] Both carbon dots and GQDs are superior in terms of chemical inertness, tunable luminescence emission, low cytotoxicity and excellent biocompatibility, long term resistance to photobleaching.[44,45] Besides, from the standpoint of health concerns and the known environmental and biological hazards of QDs, they have priority over toxic metal-based quantum dots currently in use, showing great potential as low-toxicity, eco-friendly alternatives that have the desirable performance characteristics of QDs. Though the GQDs are even considered as a kind of CDs,[46] some differences must be pointed out. The CDs are either amorphous or crystalline,[35] while GQDs are generally either produced from graphene-based starting materials or the rigid synthetic chemistry of graphene-like smaller polycyclic aromatic hydrocarbon molecules (PAHs), thus they clearly possess graphene lattices inside the dots regardless of the dot size.[9,47] Moreover, due to the size effects, luminescent CDs comprise discrete, quasi-spherical carbon nanoparticles with

Guohai Yang received his BS degree from Lanzhou University in China in 2008. Currently he is pursuing his PhD degree under the supervision of Prof. Jun-Jie Zhu at Nanjing University, China. His research interests mainly focus on the development of graphene-based composites for electrochemical applications.

Jianwei Zhao received his BS degree in 1996 (Peking University), MS in 1999 (Changchun Institute of Applied Chemistry), and PhD in 2003 (Hokkaido University). He is now a full-professor in the School of Chemistry and Chemical Engineering, Nanjing University. His research interests focus on the theoretical and experimental investigation including electrochemical engineering, theoretical simulation of nano-fabrication for Micro (Nano)-Electro-Mechanical Systems, and electron transfer through a functionalized molecule.

Juan Peng received her PhD degree with Professor Jun-Jie Zhu in Nanjing University in 2012. During her PhD candidate, she went to Rice University as a visiting student with Professor Pulickel Ajayan for one year. Currently, she is a lecturer in the School of Chemistry and Chemical Engineering at Ningxia University. Her research interests involve preparation of functional nanomaterials and their application in bioanalysis.

Jun-Jie Zhu received his BS (1984) and PhD (1993) degrees from the Department of Chemistry, Nanjing University, China. Then, he began his academic career at School of Chemistry and Chemical Engineering, Nanjing University. He entered Bar-Ilan University, Israel as a postdoctoral researcher from 1998 to 1999. Since 2001, he has been a full professor at Nanjing University. His main research activities focus on preparation and application of functional nanomaterials, and fabrication of electrochemical and electrochemiluminescence biosensors.

sizes below 10 nm.[35,48,49] Meanwhile, the GQDs are defined as the graphene sheets with lateral dimensions less than 100 nm in single-, double- and few- (3 to <10) layers.[9,49,50]

In this review, we mainly focus on the top-down synthesis of GQDs and their applications induced by fluorescent properties. Section 2 of this review summarizes the various synthetic routes to produce GQDs with emphasis on the top-down routes. In Section 3, we discuss the topography, the crystalline nature, the optical properties and their influencing factors, as well as other performances. Section 4 covers the applications of GQDs. In Section 5, we give a perspective for GQDs. We hope this article can offer valuable insight for the investigation of GQDs and further expand the boundaries of their applications.

2 Synthetic methods

Up till now, tremendous efforts have been made to develop synthetic methods for GQDs, which can be classified into two main groups: top-down and bottom-up methods. The top-down methods include electron beam lithography,[50] acidic exfoliation,[17,51,52] electrochemical oxidation,[53,54] microwave-assisted hydrothermal synthesis,[6] and so on. We can classify these methods as top-down routes where GQDs are derived from the cleavage of carbonaceous materials. In addition, GQDs can also be prepared through bottom-up routes, including the solution chemistry,[7] cyclodehydrogenation of polyphenylene precursors,[8] carbonizing some special organic precursorsor,[11,55] the fragmentation of suitable precursors, for example, the C60.[56] Some typical strategies are listed in Table 1.

The top-down routes for the preparation of GQDs have the advantages of abundant raw materials, large scale production and simple operation. Moreover, the GQDs synthesized *via* top-down methods usually contain oxygen-containing functional groups at the edge, thus facilitating their solubility, functionalization and passivation. However, this method also suffers from some disadvantages, such as the requirement of special equipment, low yield, the damage on the aromatic carbon framework, and the non-selective "top-down" chemical cutting process, which does not allow precise control over the morphology and the size distribution of the products.[9,47,55]

Conversely, the bottom-up methods offers us exciting opportunities to control the GQDs with well-defined molecular size, shape, and thus properties.[8] Nevertheless, these methods always involve complex synthetic procedures, and the special organic precursors may be difficult to obtain.[55] More importantly, the poor solubility and strong tendency of aggregation of the GQDs limits their practical applications.[9] Besides, these GQDs obtained *via* the solution chemistry are usually smaller than 5 nm, which is below the processable scale of state-of-the-art lithography technology (10 nm).[47]

In the past few years, increasing efforts have been paid to the advanced synthesis of GQDs, and the above-mentioned deficiencies have gradually overcome *via* the elaborate designs.

2.1 Top-down routes

The top-down routes are implemented *via* either physical or chemical techniques, among which the latter is in the majority.

Table 1 A brief summary of the morphologies of GQDs synthesized *via* typical synthetic methods

Methods	Subclassification	Starting materials	Size (nm)	Height (nm)	Color	Yield (%)	Ref.
Top-down	Acidic oxidation	GO	5–19		Blue		51
		GO	5–25		Blue		49
		Carbon black	15	0.5	Green	44.5	17
			18	1–3	Yellow	9.0	17
	Hydrothermal	GO	5–13	1–2	Blue	5	10
		GO	1.5–5	1.5–1.9	Green		62
		RGO	2–5		Blue		69
	Amino-hydrothermal	GO	2.5	1.13	Blue to yellow		58
	Solvothermal	GO	5.3	1.2	Green	1.6	16
		GO	3–5	0.95	Blue to Green	1.6	85
	Microwave	GO	2–7	0.5–2	Green, blue	8	6
	Microwave-hydrothermal	GO	3	<0.7	Blue		65
	Ultrasonic chemistry	Graphene	3–5		Blue		12
	Electrochemistry	Graphene	3–5	1–2	Green		53
		Graphite rods	5–10	<0.5	Yellow		54
		MWCNTs	3 ± 0.3	1–2	Green		60
			5 ± 0.3	3	Green		60
			8.2 ± 0.3	5	Green		60
			23 ± 2		Green		60
	Photo-Fenton Reaction	GO	40	1.2	Blue	45	9
	Oxygen plasma etching	Graphene	11 ± 4.3	4.5			72
	K intercalation	MWCNTs	~20	<1	Blue	22.96	61
		Graphite flakes	~20	0.9	Blue	9.9	61
Bottom-up	Stepwise solution chemistry	Organic precursors	~2.5 to 5		Red		7,8 and 97
	Precursor pyrolysis	Glucose	1.65–21	3.2	DUV, blue		11
		Citric acid	~15	0.5–2	Blue		55
	Catalyzed cage-opening	C_{60}	2.7–10			15–30	56
	Pyrolysis and exfoliation	Unsubstituted HBC	~60	2–3	Blue		47

Further, the mechanism of chemical type top-down routes can be described as defect-mediated fragmentation processes.[55,56] Namely, the oxygen-containing functional groups (epoxy and hydroxyl groups) could create defects on GO sheets and serve as chemically reactive sites, thus allowing GO to be cleaved into smaller sheets.[6,57] Generally speaking,[10,52,58,59] as shown in Fig. 1a and b, during acid oxidization of graphene, epoxy groups tend to appear linearly on a carbon lattice, and such cooperative alignment induces a rupture of the underlying C–C bonds. Once an epoxy chain appears, it is energetically preferable for it to be further oxidized into epoxy pairs that then convert to more stable carbonyl pairs at room temperature. The presence of these linear defects makes the graphitic domains fragile and readily attacked. Some ultrafine pieces, which are sub-nanometer sized aromatic sp^2 domains surrounded by the mixed epoxy lines and/or edges, may further break up to finally form the GQDs. Therefore, graphene,[10,53] GO,[6,16] and any other carbon materials consisting of aromatic sp^2 domains such as carbon fibers,[52] carbon nanotubes,[60,61] carbon black,[17] could be adopted as the starting materials for the synthesis of GQDs with the aid of hydrothermal and solvothermal treatment, acidic oxidation, electrochemical strategies, sonication and microwave assisted method, *et al.*

2.1.1 Acidic oxidation. As mentioned above, upon the oxidation treatment, GO could automatically break down into smaller parts. Li *et al.* suggested that a well-controlled oxidation induced cut of graphene could lead to more smooth edges compared to heat or sonic treatment.[59] Thus the oxidation of GO in a strong acid solution is a widely adopted method, usually followed by neutralization of the excess acid and a dialysis process.

In 2011, Shen *et al.* reported GQDs prepared by hydrazine hydrate reduction of oxidised GO with their surface passivated by polyethylene glycol (PEG).[51] Firstly, GO was further oxidized by 2.6 M HNO_3 with 70 °C reflux for 24 h to cut them into small GO sheets. After the pH was tuned to 8 with Na_2CO_3, the small GO sheets were treated with an oligomeric PEG diamine (PEG_{1500N}) as a surface passivation agent. The precursor was finally reduced by hydrazine hydration to obtain luminescent GQDs (Fig. 2a). The collected GQDs had a diameter distribution in the range of 5–19 nm (13.3 nm average diameter) and a PL quantum yield of 7.4% using rhodamine B as a reference. Strong blue PL was clearly shown under 365 nm and the green fluorescence was observed under a 980 nm laser. Later in 2012, Shen *et al.* improved the above method to obtain GQDs with enhanced fluorescence.[49] After neutralization of the excess acid, the suspension was disrupted into small pieces using an ultrasonic cell crusher for 60 min. Then using the small cut GO sheets and PEG as starting materials, GQDs-PEG were prepared by a one-pot hydrothermal reaction. The collected GQDs-PEG are nearly monodispersed with a uniform diameter of *ca.* 5–25 nm (13.0 nm average diameter). For comparison, they also prepared GQDs without the surface-passivation agent. The GQDs-PEG had the advantages of higher PL quantum yield, better upconverted PL properties and a higher photon-to-electron conversion capability compared with GQDs.

Peng and co-workers reported the synthesis of GQDs in large scale with acidic exfoliation and etching of pitch carbon fibers (CF), as shown in Fig. 2b.[52] The carbon fibers were dispersed into a mixture of concentrated H_2SO_4 and HNO_3, sonicated for two hours and stirred for 24 hours at three different temperatures (80 °C, 100 °C and 120 °C). Accordingly, three kinds of GQDs with the emission color of blue, green, and yellow were obtained, their corresponding diameters distributed between the range of 1–4 nm, 4–8 nm, 7–11 nm, respectively. The heights of the GQDs are between 0.4 and 2 nm, corresponding to 1–3 graphene layers. A clear blue shift from 330 to 270 nm with increasing the temperature was observed in the UV-visible absorption spectra, revealing that the reaction temperature

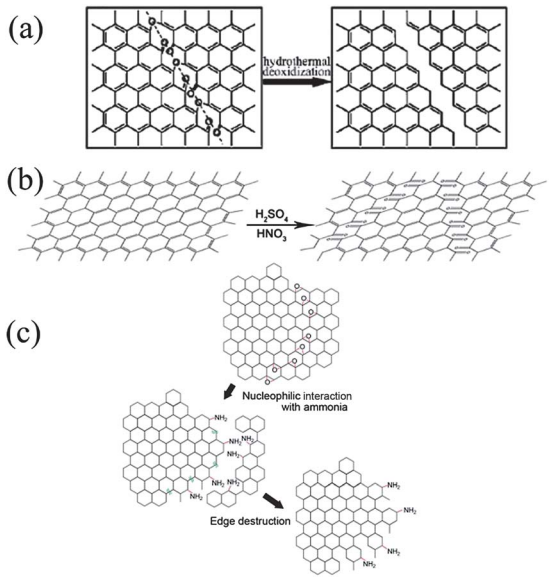

Fig. 1 (a) Mechanism for the hydrothermal cutting of oxidized GSs into GQDs: a mixed epoxy chain composed of epoxy and carbonyl pair groups (left) is converted into a complete cut (right) under the hydrothermal treatment (reprinted with permission from ref. 10. Copyright 2010). (b) Proposed mechanism for the chemical oxidation of carbon fibers into GQDs (reprinted with permission from ref. 52. Copyright 2012). (c) Schematic illustration of the proposed formation mechanism for amino-functionalized GQDs (reprinted with permission from ref. 58. Copyright 2012).

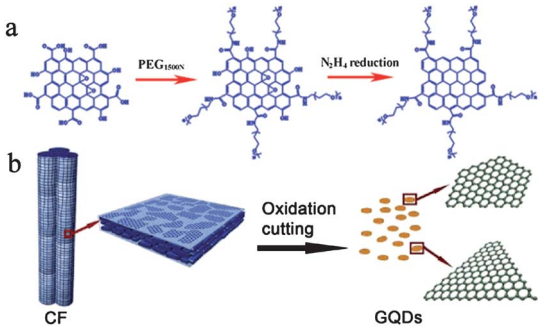

Fig. 2 (a) Representation of GQDs containing an oligomeric PEG diamino surface passivating agent (reprinted with permission from ref. 51. Copyright 2011). (b) Representation scheme of oxidation cutting of CF into GQDs (reprinted with permission from ref. 52. Copyright 2012).

could tune the size of the as-prepared GQDs and affect their absorption properties.

Acidic exfoliation is a facile process and of significance in large-scale production for broad applications of GQDs from many kinds of carbonaceous materials. However the excess amount of oxidant agent (*e.g.*, HNO_3) is difficult to be removed from the solution. Recently, Dong *et al.* reported a new facile method to prepare single- and multi-layer graphene quantum dots by chemically oxidizing CX-72 carbon black (CB) in 6 M HNO_3 under reflux for 24 h.[17] After cooling to room temperature, the suspension was centrifuged to obtain a supernatant and a sediment. The acid solution was then centrifuged to obtain a supernatant and sediment. The supernatant was heated at 200 °C to evaporate the water and nitric acid and a reddish-brown solid (GQDs1) was obtained. The GQDs1 were mostly single-layered and had an average size of 15 nm. Furthermore, the sediment suffered from routine treatments, such as washing, drying, redispersion in H_2O, in order to get the GQDs2 which were multi-layered (2–6 layers) with an average size of 18 nm. Both solutions of GQDs1 and GQDs2 emitted strong photoluminescence (PL), green and yellow respectively, under excitation at 365 nm.

2.1.2 Hydrothermal and solvothermal method. The hydrothermal method is a facile synthetic route for the preparation of GQDs. It usually required the usage of strong alkali (such as NaOH and ammonia) as scissors to cut the carbon-based precursors into colloid GQDs. In 2010, Pan *et al.* firstly reported the hydrothermal synthesis of GQDs using micrometer-sized GO sheets as the starting material.[10] Briefly, the preparation of GQDs involved the thermal reduction of monolayer GO sheets (200–300 °C for 2 h) into chemically derived graphene sheets (GSs), the oxidization of the GSs in concentrated H_2SO_4 and HNO_3 solution for 15–20 h under mild ultrasonication, and the hydrothermal deoxidation of the oxidized GSs (200 °C for 10 h) under weakly alkaline conditions (pH = 8). Their diameters are mainly distributed in the range of 5–13 nm (9.6 nm average diameter), and the topographic heights are mostly between 1 and 2 nm (1–3 graphene layers). Here, due to the low temperature for thermal de-oxidization of GO sheets and the weakly alkaline condition for the hydrothermal cutting reaction, the resultant GQDs were less ordered. Later in 2011, Pan *et al.* improved this hydrothermal approach to prepare well-crystallized GQDs using high-temperature (600 °C) thermally reduced GO sheets as the precursor by a fine chemical cutting route under strongly alkaline hydrothermal conditions (pH > 12).[62] The well-crystallized GQDs exhibited strong green fluorescence with lateral size ranging from 1.5 to 5 nm (3 nm average diameter) and a narrow height distribution from 1.5 to 1.9 nm, indicating that the GQDs typically consist of 2–3 graphene layers.

Tetsuka *et al.* reported amino-functionalized graphene quantum dots (af-GQDs) with discrete molecular weights and specific edges, extracted through the ammonia-mediated bond-scission reaction from oxidized graphene sheet.[58] As shown in Fig. 3, the oxidized graphene sheets were subjected to mild amino-hydrothermal treatment at 70–150 °C for 5 h using ammonia solution, followed by thermal annealing at 100 °C for 1 h to vapor excess ammonia. Through the nucleophilic substitution reaction with ammonia, as shown in Fig. 1c, the sp^2 domains were cut out of the sheets and appeared in the form of isolated af-GQDs by the simultaneous ring-opening of the epoxide. As a result, the af-GQDs edge-terminated with a primary amine molecule were obtained with a diameter of ~2.5 nm and a thickness of ~1.13 nm, which corresponded to single-layer of functionalized GQDs. The degree of amine functionalization, which controlled the photoluminescence color, could be controlled simply by changing the initial concentration of ammonia and the temperature of the amino-hydrothermal treatment. The af-GQDs showed a high quantum yield of 19–29% attributed to the chemical nature of af-GQDs.

A one-step solvothermal route for the preparation of strongly green-photoluminescent GQDs from GO is implemented by Zhu *et al.*[16] GO was dissolved in DMF with the concentrations of 270 mg mL^{-1}, sonicated for 30 minutes, and then heated at 200 °C for 5 h to get expected GQDs. The average diameters of GQDs was 5.3 nm, and the average height was 1.2 nm (Fig. 4), suggesting the GQDs were single layered or bi-layered. The prepared GQDs possessed strong fluorescence with PL quantum yields as high as 11.4% and could be dissolved in water and most polar organic solvents without further chemical modifications.

2.1.3 Microwave- and sonication-assisted method. Till now, most reports involve the acidic oxidation and hydrothermal methods in the synthesis of GQDs. However, these methods still have some shortcomings, for instance, the

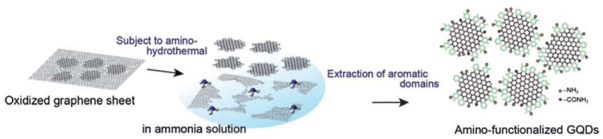

Fig. 3 Schematic illustration of the preparative strategy for af-GQDs (reprinted with permission from ref. 58. Copyright 2012).

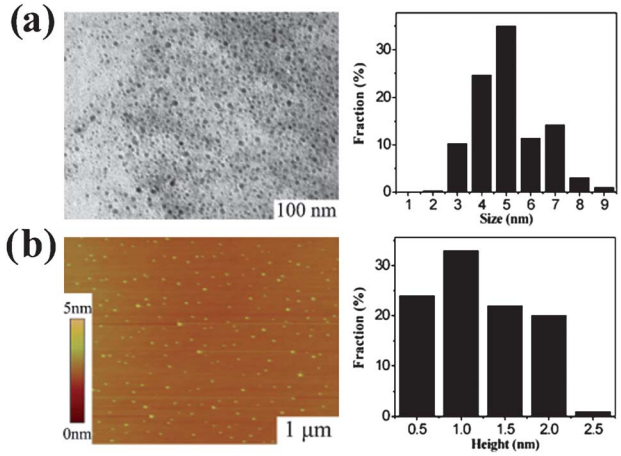

Fig. 4 Morphology of GQDs. (a) TEM image of the GQDs (average size 5.3 nm) and their size distributions. (b) AFM image of the GQDs and their height distributions (reprinted with permission from ref. 16. Copyright 2011).

long-time of the procedure. Consequently, some high-energy technologies have been adopted aiming to seek facile synthetic approaches of GQDs.

A microwave-assisted technique has been widely applied to materials synthesis for it combines both the advantages of hydrothermal and microwave techniques. As a convenient and rapid heating source, microwave assisted exfoliation and reduction of GO has been reported.[63,64] Reduced graphite oxide materials could be readily obtained in the scale of minutes and the yield of graphene prepared by this method was very high, which suggested that microwave irradiation could shorten the reaction time and improve the product yield. Recently, Li *et al.* developed a facile microwave-assisted approach for the preparation of stabilizer-free two-color GQDs from GO nanosheets under acid conditions.[6] Fig. 5 outlines the overall procedure for the preparation of GQDs. Briefly, initiated by the acid oxidation of epoxy groups, it was prone to form a mixed line on the carbon lattice composed of fewer epoxy groups and more carbonyl groups, making the graphitic domains fragile and readily attacked. The greenish yellow-luminescent GQDs (gGQDs) showed an average diameter of 4.5 nm, and were mostly single layered or bilayered. Followed by a single step of moderately reducing gGQDs with $NaBH_4$, the blue-luminescent GQDs (bGQDs) were obtained with almost the same dimension and height. The PL QYs of gGQDs and bGQDs were as high as 11.7% and 22.9%, respectively. It was also verified that reduction occurred simultaneously with the cleaving of GO, thus microwave irradiation integrated the cleaving and reduction steps into facile one step and finally simplified the synthetic process and shortened the reaction time. Later, Chen *et al.* reported an improved microwave-hydrothermal protocol at 200 °C for 5 min to prepared GQDs.[65] The as-prepared GQDs are uniform and monodispersed with an average diameter of *ca.* 3 nm. AFM images showed topographic heights of <0.7 nm, which was a clear illustration of a single-layer of the GQDs.

Ultrasonic chemical method has widely been used for the synthesis of various nanocrystals including CDs.[66,67] It is well-known that ultrasound can generate alternating low-pressure and high-pressure waves in liquid, leading to the formation and violent collapse of small vacuum bubbles. These cavitations cause high-speed impinging liquid jets, deagglomeration, and strong hydrodynamic shear-forces.[67] Thus the energy of the ultrasonic wave would favour the shearing of a carbon layered material into GQDs. Recently, Zhuo and co-workers proposed a new facile acid assisted ultrasonic method to prepare GQDs with graphene as the starting materials.[12] During the cutting process, ultrasmall particles with a protruding edge were formed. TEM images revealed the as-prepared GQDs were monodispersed with diameters of 3–5 nm.

2.1.4 Electrochemical method. Typically, carbon based materials such as graphite and MWCNTs have been widely used as the working electrode for the electrochemical preparation of CDs, as well as fluorescent graphene nanoribbons.[27,37,39] These methods adopted high redox potential, ranging from ±1.5 V to ±3 V, which was high enough to either oxidize the C–C bonds or oxidize water to generate hydroxyl and oxygen radicals playing the role of an electrochemical "scissors" in its oxidative cleavage reaction.[27] Besides, the potential cycling can drive the supporting electrolyte (BF_4^- or TBA^+ ions) to intercalate into the carbon anode (Fig. 6a), thus bring about the depolarization and expansion of the carbon anode. Both the interplay of anodic oxidation and anion intercalation lead to the exfoliation of the carbon anode and the production of CDs with the similar mechanism as mentioned in Fig. 1, namely defect-mediated fragmentation processes.[27,37,39]

This electrochemical strategy has further been extended to the production of GQDs. The electrochemical preparation of GQDs was firstly performed by Li *et al.* in 0.1 M phosphate buffer solution (PBS, pH 6.86) with a filtration-formed graphene film as the working electrode upon the application of CV scan within the potential region of ±3 V.[53] The collected GQDs were monodisperse with a uniform diameter of *ca.* 3–5 nm, the topographic heights were between 1 and 2 nm, indicating the architecture of 1–3 graphene layers. The GQDs present a green luminescence and can be retained stably in water for several

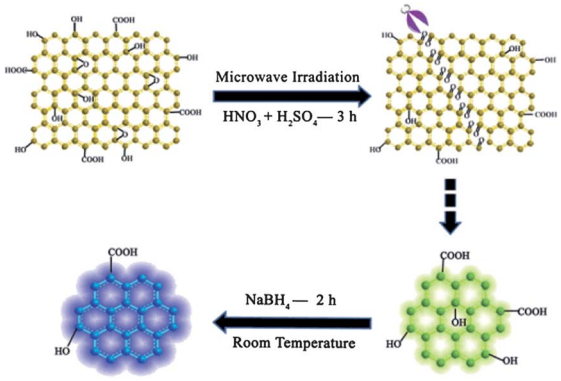

Fig. 5 Schematic representation of the preparation route for gGQDs and bGQDs (reprinted with permission from ref. 6. Copyright 2012).

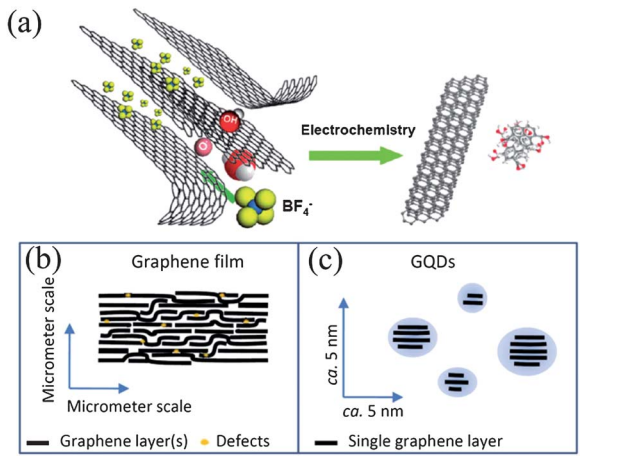

Fig. 6 (a) Illustration of the exfoliation process showing the attack of the graphite edge planes by hydroxyl and oxygen radicals, which facilitate the intercalation of BF^{4-} anion (reprinted with permission from ref. 27. Copyright 2009). (b) Scheme of the stacking structure of graphene layer(s) in filtration-formed graphene film. (c) Scheme of the electrochemically produced GQDs (not drawn to scale) (reprinted with permission from ref. 37. Copyright 2009).

months without any changes. Later in 2011, the same group used N-containing tetrabutylammonium perchlorate (TBAP) in acetonitrile as the electrolyte instead of PBS, upon the CV scanning between ±3 V, blue luminescent nitrogen-doped GQDs (N-GQDs) were obtained.[68] The N-GQDs exhibited uniform diameters of *ca.* 2–5 nm, well-consistent with electrochemically prepared N-free counterparts. The topographic height of N-GQDs is typically 1–2.5 nm, suggesting that most of the N-GQDs consist of *ca.* 1–5 graphene layers (Fig. 6c).

Zhang *et al.* prepared GQDs by electrolysis of graphite rod (GR) in alkaline condition (0.1 M NaOH) with a current intensity in the range of 80–200 mA cm^{-2}, paralleled to a Pt foil used as counter electrode.[54] The resulting solution then underwent reduction with hydrazine at room temperature to get yellow luminescent GQDs with an average diameter of 5–10 nm and a thickness <0.5 nm, mostly consisting of a single graphene layer. They found that the condition of room temperature reduction is critical to form the yellow luminescent GQDs, which will be discussed in detail in the following section.

Shinde and Pillai recently reported a two-step process for the electrochemical transformation of MWCNTs to GQDs.[60] Firstly, the MWCNT-coated working electrode in propylene carbonate with $LiClO_4$ was applied a typical anodic potential of 1 V *versus* Pt QRE (quasi reference electrode). The applied electric field initiated the breaking of sp^2 carbon atoms. Then applying a potential of −1 V *versus* QRE conduced to the intercalation of Li^+/propylene carbonate complexes which resulted in the exfoliation of oxidized MWCNTs. The mechanism was proposed in Fig. 7, assuming the vertical unzipping of MWCNTs in contrast to longitudinal unzipping in the aqueous case. This method offered a novel strategy to synthesize size-tunable GQDs by the oxidation time. By using a potential of 1 V at 90 °C for 15, 11 and 7 h resulted in GQDs with different sizes (3 ± 0.3 nm, 5 ± 0.3 and 8.2 ± 0.3 nm, respectively) and different heights (1–2 nm, 3 nm and 5 nm, respectively).

2.1.5 Other chemical routes. Attracted by the distinctive properties of GQDs, more and more alternative methods were developed in order to synthesize GQDs simply and effectively. From the above-mentioned defect-mediated fragmentation mechanism for chemical type top-down routes, it is obvious that the pre-oxide plays a key role in the synthesis of GQDs, because it introduces oxygen-containing groups and defects as reactive sites.[72] Therefore, besides the acidic oxidation and electrochemical oxidation, the seeking for effective oxidation strategies has ignited tremendous research interest. Yang *et al.* has developed a facile method to extract GQDs from reduced graphene oxide (RGO) by ozonation pre-oxide on the basis of the high oxidative capability of ozone.[69] The as-prepared GQDs was 2–5 nm in diameter, exhibited strong fluorescence activity ranging from ~355 nm to ~440 nm depending on the pH of ozonation system. It is noted that ozonation pre-oxide method is simple and efficient, low-cost, massive scalable and well controllable to obtain GQDs with different fluorescence properties.

Besides, Zhou *et al.* also demonstrated that the micrometer sized GO sheets could react with Fenton reagent (Fe^{2+}/Fe^{3+}/H_2O_2) efficiently under an UV irradiation, and, as a result, the GQDs with periphery carboxylic groups could be generated with mass scale production.[9] It has been demonstrated that H_2O_2 can be dissociated into hydroxyl radicals (·OH) under the photoassisted catalysis of Fe^{2+}/Fe^{3+} in water, and as-generated ·OH has been considered as one of the most powerful oxidizing species.[70] As shown in Fig. 8, under the UV irradiation, the produced hydroxyl radical and/or peroxide radical would attack carbon atoms connected with the hydroxyl and epoxide groups to break the C–C/C=C bonds. At the same time, the newly formed oxygen-containing groups such as the quinone group or radicals that may serve further as new photo-Fenton reaction sites. Finally, the GO sheets with micrometer lateral size were cut into small fragments. The sizes of GQDs could be controlled by varying the UV light power and photo-Fenton reaction time properly. After 15 min of the reaction, all GO sheets were cut into GQDs with an average lateral size of 40 nm, and thickness of ~1.2 nm, assuming the single atomic layer motif.

Early in 2009, Gokus *et al.* firstly discovered that PL could be induced in single-layer graphene on substrates by selective plasma oxidation.[71] Graphene sheets were exposed to oxygen/argon (1 : 2) RF plasma while only the topmost layer was affected. The PL became strong and spatially homogeneous for longer exposure times. Optical imaging at 473 nm was observed in an inverted confocal microscope. Spatially resolved PL showed bright and localized emission for short treatment times

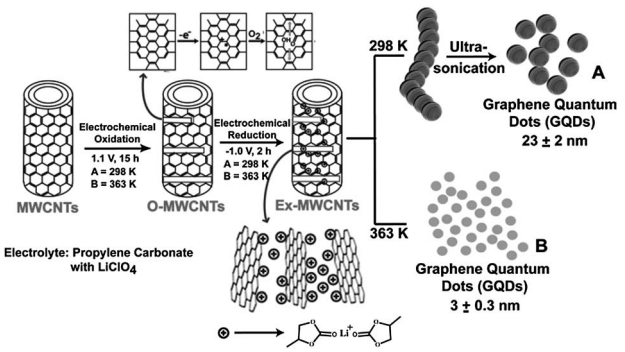

Fig. 7 Schematic representation of various processing stages involved in the preparation of photoluminescent GQDs from MWCNTs by this electrochemical approach (reprinted with permission from ref. 60. Copyright 2012).

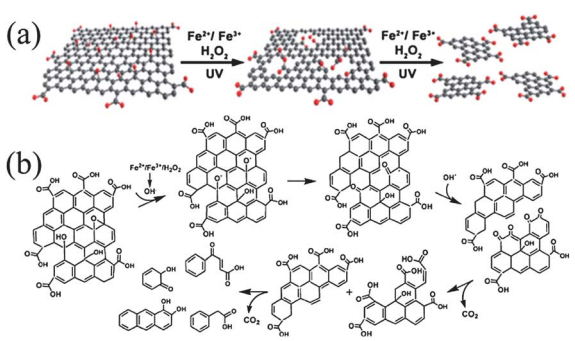

Fig. 8 (a) The scheme of the formation of GQDs. (b) Schematic representation of a proposed mechanism for the photo-Fenton reaction of the GO sheets (reprinted with permission from ref. 9. Copyright 2012).

while for longer times, the PL was strong and spatially homogeneous (Fig. 9a and b). Oxygen plasma could also be utilized for etching graphene into large area nanostructures of various materials, reported by Kim *et al.*[72] Large area arrays of graphene nanodots with tunable sizes and inter-distances were fabricated by the diblock copolymer micellar approach, which is a promising bottom-up technique for generating large area nanostructures of various materials without using sophisticated electron-beam lithography. The radius and inter-distance of fabricated graphene nanodots were 11 ± 4.3 nm and ~44 nm, respectively. An overall schematic diagram of the fabrication of an array of graphene nanodots was illustrated in Fig. 9c.

Very recently, Lin *et al.* report a novel effective approach to the preparation of water-soluble GQDs based on exfoliating and disintegrating MWCNTs and graphite flakes (GFs) respectively.[61] The preparation was based on the high reactivity of potassium–graphite intercalation compounds (K-GICs, Fig. 9d), formed by intercalating K atoms between the covalently bonded graphene sheets in MWCNTs. Upon short exposure of the K-GICs to air and the assistance of ultrasonication, the MWCNTs were exfoliated and disintegrated to yield monolayered GQDs.

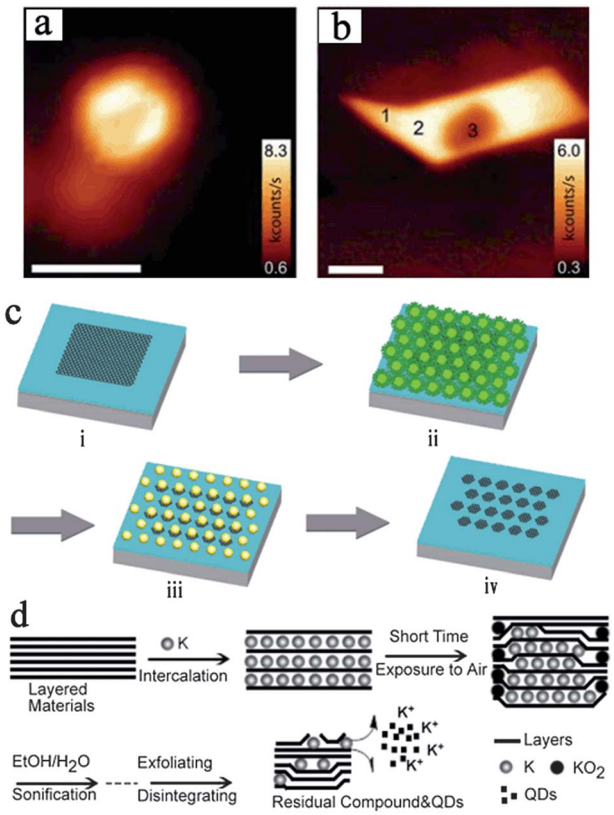

Fig. 9 (a) Confocal PL image excited at 473 nm (2.62 eV) for a graphene sample oxidized for 3 s. Scale bar = 5 μm. The bright PL spots are spatially localized. (b) Uniform emission after 5 s. Scale bar = 10 μm. For position 3 in (b), PL is bleached intentionally by intense laser irradiation (reprinted with permission from ref. 71. Copyright 2009). (c) Fabrication schematic diagram of an array of graphene nanodots: (i) graphene prepared by mechanical exfoliation of graphite powders on a SiO_2/Si substrate; (ii) a single layer of PS–P4VP micelles containing $HAuCl_4$ over the entire substrate; (iii) Au nanoparticle-protected graphene nanodots after oxygen plasma treatment; (iv) an array of graphene nanodots after the removal of Au nanoparticles (reprinted with permission from ref. 72. Copyright 2012). (d) The scheme of the formation of GQDs (reprinted with permission from ref. 61. Copyright 2012).

2.2 Bottom-up routes

Compared with the up-down routes, the reports concerning the bottom-up routes are relatively scarce. Li's group has made great effort to synthesize GQDs *via* stepwise solution chemistry based on oxidative condensation reactions.[7,8,73] The obtained large colloidal GQDs have a uniform and tunable size, containing 168, 132 and 170 conjugated carbon atoms respectively (Fig. 10a). The stabilization of the resultant GQDs was achieved by multiple 2′,4′,6′-triakyl phenyl groups covalently attached to the edges of the graphene moieties. The crowdedness on the edges of the GQDs twists the substituted phenyl groups from the plane of the core, leading to alkyl chains closing the latter in all three dimensions, as shown in Fig. 10b. This results in reduced face-to-face interaction between the graphenes, thus effectively increasing their solubility.

Some organic precursors have also shown great potential for the preparation of GQDs *via* pyrolysis or carbonization under certain conditions. Tang *et al.* firstly reported a facile microwave-assisted hydrothermal method for the production of GQDs with glucose as the starting material and also the sole reagent.[11] First the glucose molecules were dehydrated to form the nucleus of GQDs that is composed of C=C. Then the growth of GQD occurred at the spherical surface (edge growth), with increasing heating time. The source molecules reach the surface of the GQD and generate new C=C by dehydration. Owing to the high pressure induced by the hydrothermal

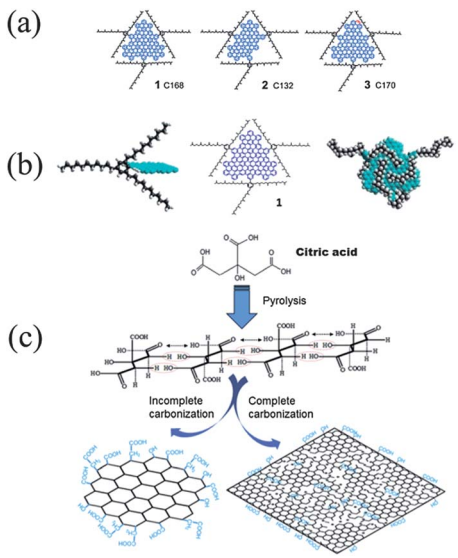

Fig. 10 (a) Schemes of colloidal GQDs with tunable size synthesized *via* stepwise solution chemistry. (b) Attaching 1,3,5-trialkyl phenyl moieties (marked black) covalently to the edge of graphene (blue) to shield the graphenes from one another in three dimensions (reprinted with permission from ref. 7 and 8. Copyright 2010). (c) Diagram for the synthesis of GQDs and GO. The black dots in the GO represent oxygen atoms (reprinted with permission from ref. 55. Copyright 2012).

condition, the freshly formed C=C is orderly arranged and assists the growth of crystalline GQDs. The diameter of the GQDs can be increased by increasing microwave heating time. The size of the GQDs can be tuned from 1.65 to 21 nm by simply prolonging the heating time from 1 to 9 min. at the same time. They also claimed that most of the carbohydrates which contain C, H, and O in the ratio of ~1 : 2 : 1 may be used as the carbon source to prepare GQDs. At the same time, Dong *et al.* prepared blue luminescent GQDs as well as GO by tuning the carbonization degree of citric acid, as depicted in Fig. 10c.[55] The GQDs are sheet like with ~15 nm in width, and 0.5–2.0 nm in thickness (1.4 nm average height). It was confirmed that the GQDs were well surface-passivated by the incompletely carbonized citric acid.

Loh *et al.* reported a mechanistic approach to the synthesis of a series of geometrically well-defined GQDs on a ruthenium surface using C_{60} molecules as a precursor.[56] It has been demonstrated that the structures are formed through the ruthenium-catalysed cage-opening of C_{60}, the strong C_{60}–Ru interaction induced the formation of surface vacancies in the Ru single crystal and a subsequent embedding of C_{60} molecules in the surface. The fragmentation of the embedded molecules at elevated temperatures then produces carbon clusters that undergo diffusion and aggregation to form GQDs.

Larger sized GQDs (~60 nm) with uniform morphology have also been obtained by Liu *et al.* using unsubstituted hexa-*peri*-hexabenzocoronene (HBC) as the carbon source following a process of carbonization, oxidization, surface functionalization with PEG_{1500N}, and reduction with hydrazine.[47] The thickness of the acquired GQDs was 2–3 nm, suggesting that they contained more than one layer of graphene. These GQDs are the largest GQDs reported so far.

3 Physical and chemical properties

3.1 Morphology, component and crystalline nature

3.1.1 Morphology. The morphology of the GQDs, including the size and height, are summarized according to the synthetic strategies as shown in Table 1. Obviously, the sizes of GQDs are largely irrelevant to the preparation methods, but independent of the starting materials. For instance, with GO as the starting materials, Pan *et al.* prepared two kinds of GQDs with average size of 9.6 nm and ~3 nm respectively, just by adopting different thermal reduction temperature and hydrothermal deoxidation alkalinity.[10,62] However, in general, the average sizes of GQDs are mostly below 10 nm, and the largest diameter of GQDs reported so far is 60 nm.[47] Similar to the size, the height also depends on the preparation methods. The heights of GQDs prepared through the same methods increase upon the increasing sizes. However, the heights of GQDs prepared through different methods don't monotonously relate to their sizes, namely, larger sized GQDs may be thinner than small sized ones. For example, the GQDs prepared *via* electrochemical method with average sizes of 3 ± 0.3 nm, 5 ± 0.3 nm and 8.2 ± 0.3 nm exhibited topographic heights of 1–2 nm, 3 nm, and 5 nm, respectively.[60] But GQDs synthesized through K-GICs showed diameter and height of ~20 nm and 0.9 nm, respectively.[61] On the whole, most of GQDs consist of no more than 5 layers, and a great deal of monolayer GQDs have been prepared till now.[9,17,54,61,65]

3.1.2 Component. Technically speaking, GQDs are only composed of elemental C and H. However, limit by their strong tendency for aggregation due to the face-to-face attraction and the preparation methods such as oxidation derived exfoliation, GQDs reported so far are always partially oxidized, with hydroxyl, epoxy/ether, carbonyl and carboxylic acid groups on the surfaces.[16,53] Fourier transform infrared (FTIR) and X-ray photoelectron spectroscopy (XPS) spectra are commonly adopted to analyze their component. For the GQDs prepared from carbon fibers (CF) *via* acidic oxidation,[52] as shown in Fig. 11, the XPS spectra showed a dominant graphitic C1s peak at 284.8 eV and O1s peak at *ca.* 532 eV for original CF and GQDs. The comparison of the high-resolution spectra of C1s demonstrated the obvious change in carbon chemical environment from CF to GQDs. The presence of C=C, C–O, C=O, and COOH bonds indicated that GQDs were functionalized with hydroxyl, carbonyl, and carboxylic acid groups. In the FTIR spectra, the introduction of oxygen-containing groups, including carbonyl, carboxyl, hydroxyl, and epoxy groups during the oxidation was quite obvious. Similar results were also observed from GQDs fabricated *via* other methods.[9,16,53,54,60,61,74] The O/C atomic ratio has also been obtained from XPS spectra to evaluate the oxidation level of GQDs. For instance, the O/C atomic ratio for GQDs prepared through hydrothermal method was 66.23%, much high than 39.22% for the original GO.[74] The O/C atomic ratio for GQDs *via* electrochemical cutting was 27%, higher than that of the graphene film (*ca.* 15%).[68] And compared with CF (~13.3%), the resulting GQDs showed a much higher O/C atomic ratio of about 23.7%.[52] Elemental analysis has also been used to characterize GQDs prepared *via* citric acid carbonization.[55] The C, H and O contents (wt%) for GQDs are 46.22%, 3.87% and 49.91% respectively, and for citric acid are 34.29%, 4.76%, and 60.95. The higher carbon contents of GQDs implied the carbonization of citric acid.

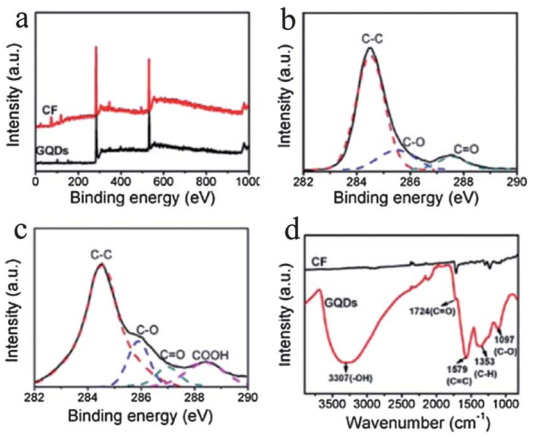

Fig. 11 (a) XPS survey spectrum of CF and GQDs. (b) High-resolution XPS C1s spectra of CF. (c) The XPS C1s spectra of GQDs. (d) FTIR spectra of CF and GQDs (reprinted with permission from ref. 52. Copyright 2012).

3.1.3 Crystalline nature. The crystalline nature of GQDs can be investigated through X-ray diffraction (XRD) patterns, Raman spectroscopy and high resolution transmission electron microscopy (HRTEM) observations. Both (002) interlayer spacing and (100) in-plane lattice spacing exist in GQDs, and the former has been widely studied. The interlayer spacing of GQDs depends strongly on their oxidation degree, that is, the attached hydroxyl, epoxy/ether, carbonyl and carboxylic acid groups can increase the interlayer spacing of GQDs. For XRD patterns, GQDs prepared by using unsubstituted HBC as the carbon source showed well-defined wide-angle XRD pattern, with the peaks respectively corresponding to the (002), (100), (004), and (110) planes (Fig. 12a), indicating their high degree of crystallinity.[47] However, GQDs prepared *via* other methods only feature a broad (002) peak around 25° (0.34 nm), which is often broad due to the small size of GQDs (Fig. 12b).[54] This difference can be ascribed to the big diameter of unsubstituted HBC derived GQDs, which is 60 nm, the largest GQDs reported so far. The exact interlayer spacing can vary according to the preparation methods. GQDs prepared through electrochemical cutting from graphene film, citric acid carbonization showed an interlayer spacing of about 0.34 nm, close to that of bulk graphite (0.334 nm[53–55,68]). Nevertheless, GQDs derived from CF had a much larger interlayer spacing of 0.403 nm, which could be attributed to the oxygen-containing groups introduced in the exfoliation and oxidation of CF.[52] The two kinds of GQDs, GQDs1 and GQDs2, showed (002) peak centered at 22.1° and 23.0° respectively, owing to the different oxygen content.[17] The GQDs synthesized by the carbonization of glucose showed spacing ranging from 0.343 to 0.481 nm.[11] The N-GQDs *via* hydrothermal treatment of graphene oxide in the present of ammonia showed 0.393 nm interlayer spacing,[74] and the GQDs-PEG *via* hydrothermal reaction had an (002) interlayer spacing of 0.381 nm due to the surface-passivation by PEG.[49] It is noteworthy that the oxygen-containing groups can expand the space of graphene layers, but sometimes highly oxidized GQDs may have smaller interlayer spacing than that of GQDs with lower oxygen content. For instance, the O/C atomic ratio and interlayer spacing for CF derived GQDs are 23.7% and 0.403 nm, respectively.[52] However, the electrochemically synthesized GQDs with higher O/C atomic ratio (27%) showed smaller interlayer spacing of 0.34 nm.[68] For another example, the N-GQDs prepared *via* hydrothermal treatment, together with the GO and RGO, showed O/C atomic ratios of 66.23%, 39.22%, and 12.09%, but their interlayer spacing are 0.393, 0.852, and 0.363 nm, respectively.[74] This phenomenon can be explained by the position of oxygen-containing groups on the graphene sheets, namely the oxygen-containing groups distributed on the basal plane can lead to larger spacing than that at the edges of graphene sheets.

The Raman technique is also a powerful and non-destructive tool for the characterization of GQDs. The G band is assigned to the E_{2g} vibrational modes of the aromatic domains, whereas the D band arises from the breathing modes of the graphitic domains. Traditionally, the intensity ratio of "disorder" D to crystalline G (I_D/I_G) is used to compare the structural order between crystalline and amorphous graphitic systems. The I_D/I_G values of GQDs vary significantly depending on the preparation methods. The electrochemically prepared GQDs from graphene film exhibited small I_D/I_G value of 0.5 (Fig. 12c), indicating not only the high quality of as-prepared GQDs, but also the uniqueness of the electrochemical method for GQD preparation.[53] But the electrochemically prepared GQDs from high purity graphite rods have higher I_D/I_G value of 0.91, the same value was also observed from CF derived GQDs.[52,54] Such a large ratio indicated defects of the GQDs with a partially disordered crystal structure, arising from the small sp^2 cluster size.[54] N-GQDs prepared by both hydrothermal and electrochemical treatment have I_D/I_G value of ~0.7, suggesting the relatively high quality of GQDs.[68,74] Besides, much higher I_D/I_G values have also been obtained from GQDs prepared by electrochemical method from MWCNTs,[60] hydrothermal cutting method,[62] and ozonation pre-treated method,[69] which are 1.23, 1.47, and 1.27–1.48, respectively, indicating the decrease of the fraction of the sp^2 domains and different degrees of GQDs oxidation, as well as an increase of the number of defect sites.

The HRTEM images of GQDs features two kinds of lattice fringes, namely (002) interlayer spacing and (1120) in-plane lattice spacing. Similar to the XRD pattern, the former centered at about 0.34 nm has been observed from GQDs prepared by acidic oxidation from carbon black,[17] microwave-assisted method,[6] and electrochemical cutting method.[68] The in-plane lattice spacing mostly centered at about 0.24 nm has been observed from GQDS synthesized *via* microwave-hydrothermal protocol,[65] amino-hydrothermal method,[74] K intercalation,[61] acidic oxidation from carbon fibers,[52] and photo-Fenton reaction,[9] excepting that valued at about 0.21 nm *via* hydrothermal cutting strategy and glucose carbonization method.[11,62] Besides, these two kinds of lattice fringes have been simultaneously been observed in the case of electrochemical method from MWCNTs

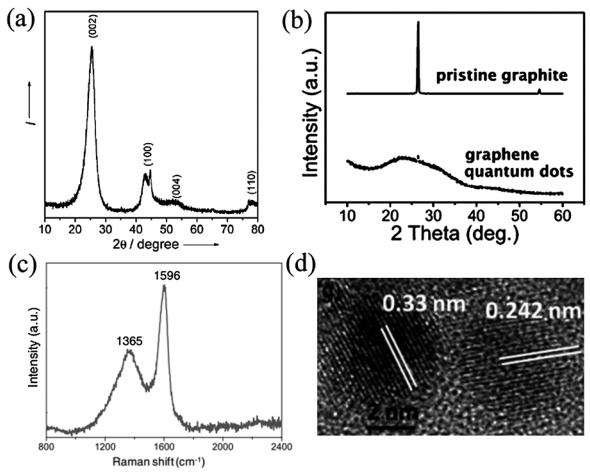

Fig. 12 (a) Wide-angle XRD pattern of GQDs prepared from unsubstituted HBC (reprinted with permission from ref. 47. Copyright 2011). (b) XRD patterns of the pristine graphite and GQDs prepared *via* electrochemical method (reprinted with permission from ref. 54. Copyright 2012). (c) Raman spectra of as-prepared GQDs *via* electrochemical method from graphene film (reprinted with permission from ref. 53. Copyright 2011). (d) Fringe patterns of GQDs prepared *via* electrochemical method from MWCNTs (reprinted with permission from ref. 60. Copyright 2012).

and acidic oxidation from natural graphite,[54,60] as shown in Fig. 12d. Moreover, GQDs are not always crystalline, amorphous GQDs has also been prepared *via* hydrothermal method and citric acid carbonization.[49,55]

3.2 Optical properties

3.2.1 Absorption. GQDs typically show strong optical absorption in the UV region, with a tail extending out into the visible range. For the UV-vis absorption spectrum of a GO sample, two kinds of peaks can been seen: a peak at ~230 nm due to π–π* transition of aromatic C=C bonds, and a shoulder at ~300 nm assigned to n–π* transition of C=O bonds.[75] In the case of graphene, the π–π* transition peak shifts to ~270 nm with the disappearance of n–π* transition peak.[76] These peaks can also be observed in the UV-vis absorption spectra of GQDs, with the π–π* transition peak centered at a wavelength between 200 and 270 nm and the n–π* transition peak at wavelength longer than 260 nm,[17,54,61,77] as shown in Fig. 13a. Sometimes the former is not distinguishable, probably because of the screening of the strong background absorption.[10,12,16,53,58,68] Due to the quantum confinement effect, the UV-vis spectra of GQDs revealed size dependent optical absorption. As shown in Fig. 13b, for the CF derived GQDs, the absorption peak red-shifted from 270 nm to 330 nm with increasing the size from 1–4 nm to 7–11 nm.[52] The hydrothermally prepared GQDs also showed the same size dependence, with varying the average size of GQDs from 5 to 35 nm, the peak energy of the absorption spectra monotonously decreases (Fig. 13c).[78] This is consistent with other QDs with quantum confinement effect.[79] However, for the GQDs prepared *via* glucose carbonization, the two absorption peaks were independent of the size even though the size increased from 1.65 to 21 nm (Fig. 13d).[11] Moreover, GQDs prepared *via* different methods also showed different absorption behaviors. For instance, the citric acid carbonized GQDs (~15 nm) had an absorption band of 362 nm,[55] but the unsubstituted HBC derived GQDs with size of about 60 nm only showed a weak shoulder at 280 nm.[47] Thus the absorption peak position was also dependent on the preparation method. Besides, the variation of oxygen content was reported to play important role in deciding the absorption peak position of GQDs.[69]

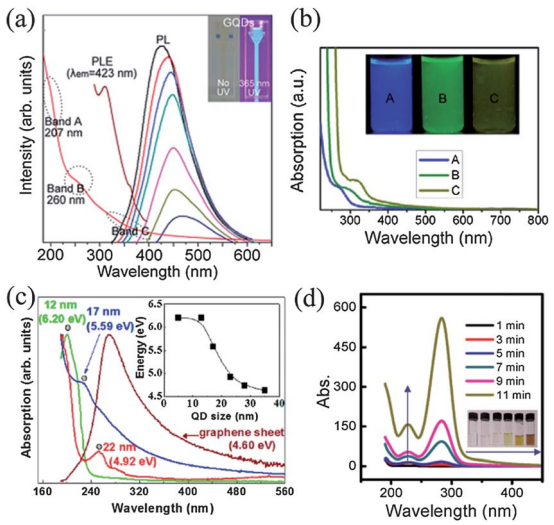

Fig. 13 (a) UV, PL and PLE spectra of GQDs created from graphite flakes (reprinted with permission from ref. 61. Copyright 2012). (b) UV-vis spectra of GQDs A, B, and C, corresponds to synthesized reaction temperature at 120, 100, and 80 °C, respectively (reprinted with permission from ref. 52. Copyright 2012). (c) Absorption spectra for three typical GQDs of 12, 17, and 22 nm average sizes dispersed in DI water and a graphene sheet. Filled circular dots indicate the peak positions of the absorption spectra for GQDs. Inset: absorption peak energy as a function of average GQD size (reprinted with permission from ref. 78. Copyright 2012). (d) The effect of microwave heating time on the absorbance of the GQDs prepared at 595 W (reprinted with permission from ref. 11. Copyright 2012).

3.2.2 Photoluminescence

3.2.2.1 Photoluminescence mechanism. For both CDs and GQDs, one of the most fascinating features is their photoluminescence. Till now, variously sized CDs with different PL colors, ranging from the visible into the near-infrared region, have been prepared *via* various synthetic approaches. However, the exact mechanism of PL for CDs remains unsettled.[34,35] The luminescence has been tentatively suggested to arise from excitons of carbon, emissive traps, quantum confinement effect, aromatic structures, oxygen-containing groups, free zigzag sites and edge defects.[34,38,39,80–84] A widely accepted mechanism for luminescence emission from CDs needs systematic investigation.

As shown in Table 1, GQDs prepared *via* different approaches can emit PL with different colors, including DUV,[11] blue,[9,10,12,49,51,61,65,69] green,[6,16,17,53,62,85] yellow,[17,54,58] and red.[8] However, similar to CDs, the PL mechanism of GQDs is still a matter of current debate and requires further clarification. Typically, the luminescence mechanism may derive from intrinsic state emission and defect state emission.[13] The former is induced by either quantum size effect,[16,53] zigzag edge sites[10,52] or recombination of localized electron–hole pairs,[19,57] while the latter arises from defect effect (energy traps).[9,16,49] All these potential mechanisms show a high level of convergence with that for CDs as listed above.

As mentioned in the introduction section, GQDs exhibit extraordinary quantum confinement and edge effects, which can play an important role in the PL of GQDs. Fig. 14a shows an energy gap of π–π* transitions calculated based on density functional theory (DFT) as a function of the number of fused aromatic rings (*N*).[19] We can see that the band gap depends on the size of the graphene fragments and generally it decreases with the increase of the size. Such size effect can result in varying PL emission with different sized GQDs. Moreover, when the graphene sheets are cut along different crystallographic directions, types of edges (armchair and zigzag edges) can be obtained. The edge type plays an important role in determining the electronic, magnetic, and optical properties.[86] Ritter and Lyding have stated that predominantly zigzag-edge GQDs with 7–8 nm average dimensions are metallic owing to the presence of zigzag edge states, and GNRs with a higher fraction of zigzag edges exhibit a smaller energy gap than a predominantly armchair-edge ribbon of similar width.[87] Kim *et al.*[78] demonstrated that circular/elliptical GQDs consist of both zigzag and armchair edges, but polygonal GQDs consist mostly of armchair

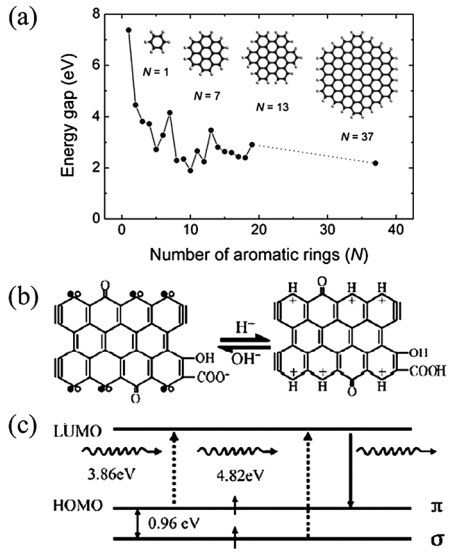

Fig. 14 (a) Energy gap of π–π* transitions calculated based on DFT as a function of the number of fused aromatic rings (*N*). The inset shows the structures of the graphene molecules used for calculation. (b) Models of the GQDs in acidic (right) and alkali (left) media. The two models can be converted reversibly depending on pH. The pairing of σ (●) and π (○) localized electrons at carbene-like zigzag sites and the presence of triple bonds at the carbyne-like armchair sites are represented. (c) Typical electronic transitions of triple carbenes at zigzag sites of GQDs (reprinted with permission from ref. 19. Copyright 2010).

edge. GQDs with size of ~10 nm have circular periphery with typical zigzag edges, and a circular-to-polygonal-shape and corresponding edge-state variations (from zigzag to armchair) of GQDs could be seen as the GQD size increased. Radovic and Bockrath reported that the zigzag sites are carbene-like, with a triplet ground state being most common, whereas the armchair sites are carbyne-like, with a singlet ground state most common.[88] Hydrothermally cut GQDs (9.6 nm average diameter) prepared by Pan *et al.* showed PL originating from free zigzag sites with a carbene-like triplet ground state, the blue emission is the irradiation decay of activated electrons from the LUMO to the HOMO,[10] the detailed mechanism is illustrate in Fig. 14c.

As discussed above, GQDs reported till now mostly have some oxygen-containing functional groups, such as hydroxyl, epoxy/ether, and carbonyl and carboxylic acid groups. In luminescent GO sheets, the presence of isolated small (2–3 nm) sp^2 clusters isolated within the sp^3 C–O matrix leads to the localization of electron–hole pairs, facilitating radiative recombination of small clusters.[19,57] These functional groups can also lead to the formation of "surface states" on GQDs, which are the energy levels between π and π* states of C=C. The functional groups have various energy levels, which may result in a series of emissive traps. When a certain excitation wavelength illuminates the GQDs, a surface state emissive trap will dominate the emission.[11] And a higher degree of surface oxidation can result in more surface defects, resulting in the red-shifted emission.[85,89]

In general, PL of GQDs is attributed to either combining effect or competition between intrinsic state emission and defect state emission. GQDs prepared *via* various methods probably exhibit distinct PL mechanism, which leads to different dependences of their PL on size, excitation wavelength, pH, solvent, *etc.*

3.2.2.2 Size dependence. A major feature of quantum dots is the quantum confinement effect, which occurs when quantum dots are smaller than their exciton Bohr radius.[90–92] And the most important consequence of such effect is the size dependence of the band gap for quantum dots, giving rise to unique, size-dependent optical and spectroscopic properties.[92,93] Typically, as the particles are smaller, the luminescence energies are blue-shifted to higher energies.[94] Both CDs and GQDs are reported to exhibit quantum confinement effect. Li *et al.* provided definitive evidence for the quantum confinement effect and size-dependent optical properties of CDs prepared by alkali-assisted electrochemical method.[38] They purified and separated the as-synthesized CDs to obtain different-sized CDs with a narrow size distribution by simple column chromatography. Further characterization supported the conclusion that the PL properties vary sharply with CDs size: small CDs (1.2 nm) give UV light emission, medium-sized CDs (1.5–3 nm) give visible light emission, and large CDs (3.8 nm) give near-infrared emission.

Similar to CDs, GQDs also exhibits size-dependent PL mainly attributed to the quantum confinement effect. Peng *et al.* prepared three kinds of GQDs with different sizes of 1–4 nm (A), 4–8 nm (B), 7–11 nm (C) *via* varying the reaction temperatures, which emitted different PL changing from blue and green to yellow as shown in Fig. 13b.[52] GQDs prepared *via* acidic oxidation from carbon black showed PL transition from green to yellow as their sizes increased from 15 to 18 nm.[17] Nevertheless, similar to what has been observed in absorption spectra, size-dependent PL might not reflect the whole story. Size-independent PL could also been observed from GQDs prepared *via* glucose carbonization, which also showed size-independent absorption spectrum as discussed above, possibly because the surface state emission played the predominant role in their PL mechanism.[11] Moreover, as shown in Table 1, the emission colors of GQDs prepared *via* different methods were contrary to what would be expected based solely on quantum confinement effects, namely, smaller GQDs had longer emission wavelength, and larger GQDs exhibited shorter one. Thus, the PL peak position was also dependent on the preparation method. Such phenomenon has also been observed for CDs.[34,35] This can be ascribed to the fact that the PL mechanism of GQDs is complicated, and besides the quantum size effect, the zigzag edge sites and defect effect (energy traps) also play important roles. In addition, apart from the particle size, the quantum confinement effect is also influenced by the composition, internal structure, and shape.[92,95] Consequently, the size performs a role in deciding the GQDs PL, but it is not the sole determinant.

3.2.2.3 Excitation dependence. The excitation wavelength dependence of the emission wavelength and intensity is a common phenomenon observed in carbon-based fluorescent materials.[23,35] They afford multi-PL colors under different excitation wavelengths and this property is important for certain

practical applications.[13] For CDs, the excitation-dependent PL behaviors may reflect not only effects from particles of different sizes in the sample, but also a distribution of different emissive sites on each carbon dot.[34,35] Unquestionably, excitation-dependent PL behaviors could also been observed in most of GQDs,[16,47,51,52,69,74] as shown in Fig. 13a and 15a. When GQDs prepared *via* solvothermal method were excited at wavelengths from 400 to 540 nm, the PL peak shifted from 515 nm to 570 nm and the PL intensity decreased remarkably.[16] Analogous to CDs, this excitation dependence properties may result from optical selection of differently sized GQDs and/or different emissive sites on GQDs.[16,33,60,89] Thus the excitation-independent behavior is probably obtainable when the GQDs have uniform size and emissive sites, or they share PL mechanism different from the above-mentioned ones. Surely, the as expected excitation-independent PL has been reported.[12,54,55] For instance, as shown in Fig. 15c, GQDs prepared *via* citric acid pyrolysis[55] have the maximum excitation wavelength and the maximum emission wavelength at 362 and 460 nm, respectively. And when the excitation wavelength changed from 300 to 440 nm, the PL spectra were almost invariable. This could be explained by the high uniformity both in the size and the surface state of those sp^2 clusters contained in GQDs which was responsible for the PL of GQDs in this case.

3.2.2.4 pH dependence. The PL of some GQDs is also pH-dependent. Under alkaline conditions, the hydrothermally prepared GQDs by Pan *et al.* emitted strong PL whereas, while under acidic conditions, the PL was nearly completely quenched.[10,62] If pH value was switched repeatedly between 12 (or 13) and 1, the PL intensity varied reversibly, which is depicted in Fig. 15d. Here, it is noteworthy that the pH had nearly no influence on the PL wavelength, but just affected obviously the PL intensities of GQDs. Similar behaviors have been commonly observed in GQDs with emissive zigzag sites.[52,69,74] The reversible phenomenon was interpreted in Fig. 14b, based on the proposed structural models. Under acidic conditions, the free zigzag sites of the GQDs were protonated, forming a reversible complex between the zigzag sites and H^+. Thus the emissive triple carbene state was broken and became inactive in PL. However, under alkaline conditions, the free zigzag sites were restored, thereby leading to the restoration of PL. However, this kind of pH dependence is not always the case. GQDs synthesized *via* solvothermal method had another interesting pH-dependent PL behavior:[16,85] PL intensities decreased in a solution of high or low pH, but remained constant in a solution of pH 4–8. Moreover, in an alkaline solution, the PL peak of the GQDs blue-shifted and the FWHM became narrow, suggesting that the PL mechanism was not the same as emissive free zigzag sites. PEG passivated GQDs exhibited bright PL in a water solution of neutral pH, and the intensity of PL peaks decreased by about 25% under both acidic and alkaline conditions.[51] Moreover, GQDs reported by Dong *et al.* showed the strongest PL intensities in weakly acidic solutions (pH 4–6) and decreased under alkaline conditions, indicating a different mechanism from the emissive free zigzag sites.[17]

The incoherence in pH-dependent PL behaviors clearly indicates dissimilar PL mechanisms in different GQDs, but the definite interpretation is still in abeyance. These pH dependent PL properties, except the zigzag edges derived ones, may be due to the emissive traps on GQDs surface. This speculation is supported by the report that the alkylamines modificated GQDs (m-GQDs) and $NaBH_4$ reduced GQDs (r-GQDs) had unchanged PL upon the variation of pH value from 0 to 14, while that changed significantly in high pH range in free GQDs (Fig. 16a). Probably because only defect state emission was highly susceptible to environment changes while the intrinsic state emission was not.[13]

3.2.2.5 Solvent dependence. The GQDs are highly soluble in water and most polar organic solvents because of the oxygen-containing functional groups on GQDs.[52] The GQDs synthesized *via* solvothermal method had solubility over 15 mg mL^{-1} in tetrahydrofuran (THF), acetone, DMF, dimethyl sulfoxide (DMSO), ethanol and water.[16] The PL of this kind of GQDs is also demonstrated to be sensitive to the species of solvent. As shown in Fig. 15b, the PL peak shifted from 475 to 515 nm in THF, acetone, DMF, water, respectively. Similar to the pH-dependent case, this phenomenon could also be ascribed to the defect state, as the r-GQDs and m-GQDs exhibited negligible solvent-dependent behaviors (Fig. 16b).[13] The GQDs prepared *via* acidic oxidation from GO also showed solvent-dependent PL, which was induced by a lone electron pair which changed the electron state of GQDs and could affect fluorescence.[96]

3.2.2.6 Concentration dependence. Besides, the concentration of GQDs sometimes can also affect their PL properties, either the wavelength or the intensity. Chen *et al.* reported the self-assembled aggregation of GQDs prepared by a

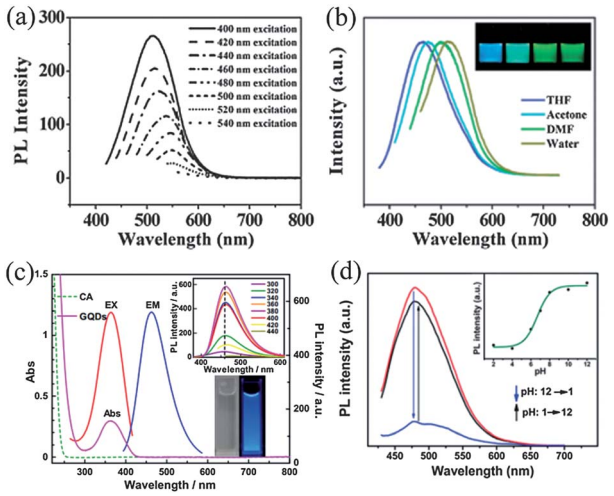

Fig. 15 (a) The excitation-dependent PL behavior of GQDs. (b) Effect of solvents on the fluorescence of GQDs (at 375 nm excitation). From left to right, the solvents are THF, acetone, DMF, water, respectively, inset: photograph of the four dispersions taken under UV light (reprinted with permission from ref. 16. Copyright 2011). (c) UV-vis absorption of citric acid (CA) and the GQDs, and PL spectra of the GQDs. Inset: (upper) emission spectra of the GQDs with excitation of different wavelength; (lower) photographs of the solution of GQDs taken under visible light (left) and under 365 nm UV light (right) (reprinted with permission from ref. 55. Copyright 2012). (d) pH-dependent PL spectra when pH is switched between 12 and 1; inset: dependence of PL intensity on pH varied from 12 to 2. (reprinted with permission from ref. 62. Copyright 2012).

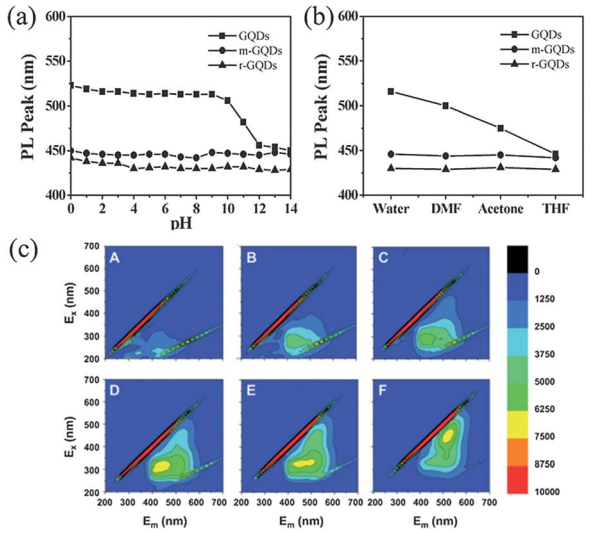

Fig. 16 (a) pH-dependent PL of GQDs, m-GQDs, and r-GQDs. (b) solvent-dependent PL of GQDs, m-GQDs, and r-GQDs (reprinted with permission from ref. 13. Copyright 2012). (c) 2D-Fluorescence topographical map of GQDs aqueous solution at different concentrations (mg mL^{-1}). (A) 0.01, (B) 0.05, (C) 0.1, (D) 0.2, (E) 0.33, (F) 1.0 (reprinted with permission from ref. 66. Copyright 2012).

microwave-assisted hydrothermal method.[65] A few single GQDs with a primary average diameter of *ca.* 3 nm gathered head-to-tail with partial overlapping into larger GQDs aggregated with a size of 20–30 nm. The increase of GQDs concentration resulted in a red-shift of the emission maximum due to the self-assembled J-type aggregation. At 1.0 mg mL^{-1} GQDs concentration, the emission and excitation maximum shifted to 525 nm and 480 nm, respectively (Fig. 16c). Pan *et al.* also studied the dependence of PL intensity on the concentration of GQDs aqueous dispersions.[62] For low concentrations (absorbance less than 0.3), a linear dependence was observed, but with increasing the concentration to absorbance larger than 0.6, PL intensity was unvaried.

3.2.2.7 Quantum yield. The quantum yield (QY) of GQDs varies with the fabrication method and the surface chemistry involved. As for the unpassivated GQDs, their QYs ranged between 2% and 22.9%, which are observed in GQDs prepared *via* stepwise solution chemistry and microwave-assisted acidic oxidation, respectively.[6,97] The GQDs commonly contains carboxylic and epoxide groups, which can act as the non-radiative electron–hole recombination centers.[57] Therefore, the removal of these oxygen-containing groups maybe improves the QY, either by reduction or surface passivation.[6,49] Shen *et al.* prepared GQDs-PEG with QY as high as 28.0%, which was two times higher than the GQDs (*ca.* 13.1%).[49] This improvement probably originates from the stabilization effect of excitons in the GQDs after passivation by PEG.[35,98] Li *et al.* improved the QY of GQDs from 11.7% to 22.9% by gentle reduction with $NaBH_4$.[6] The m-GQDs and r-GQDs proposed by Zhu *et al. via* alkylamine modification and reduction showed substantially increased QY (6.5% and 12.1%, respectively) in comparison with that of free GQDs (5.9%).[13] In addition, Tetsuka *et al.* prepared amino-functionalized GQDs (af-GQDs) with QYs ranging from ~29 to 19%, which decreased with quantity of amine functionalization.[58] More importantly, significantly enhanced QY of ~46% could be obtained *via* further passivating the af-GQDs with PEG, which is the highest value for QDs reported so far.

3.2.3 Upconversion luminescence. In addition to the strong downconversion PL properties, remarkably, some of the GQDs show a clear upconversion PL feature, firstly reported by Shen *et al.* in 2011.[51] They found that, for PEG passivated GQDs prepared *via* acidic oxidation, when the excitation wavelength changed from 600 to 800 nm, the upconverted emissions peaks shifted from 390 to 468 nm, respectively (Fig. 17a). Remarkably, the shifting between the energy of upconverted emission light (E_m) and excitation light (E_x) was almost unchanged, about 1.1 eV. They speculated the upconversion PL as an anti-Stokes transition as depicted in Fig. 17b, where the energy levels of p and s orbitals were provided by the carbine ground-state multiplicity. When a bunch of low-energy photons excite the electrons of the π orbital, the π electrons would be excited to a high-energy state such as the LUMO. And then the electrons relax back to a low-energy state, leading to the upconverted PL emitting. Although the electrons of the σ orbital can also be excited, they only can emit normal PL. The same anti-Stokes transition induced upconversion PL was also observed from GQDs-PEG prepared by a one-pot hydrothermal reaction.[49] Zhu *et al.* also observed upconversion PL from GQDs prepared *via* solvothermal method,[13,84] As shown in Fig. 17c, when excited from 600–900 nm, the emissions red-shifted significantly, and the upconversion PL was attributed to the multiphoton active process, similar to previous reported CDs.[13,85] Moreover, excitation-independent upconversion PL property has been reported by Zhuo *et al.* from ultrasonically synthesized GQDs (Fig. 17d).[12]

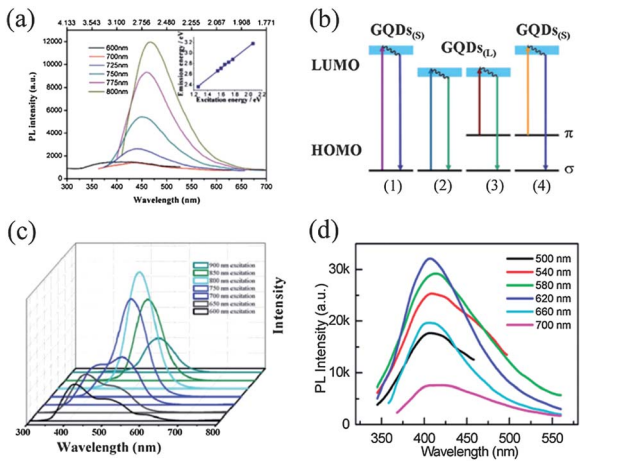

Fig. 17 (a) Upconverted PL properties of GQDs, inset is the energy of the excitation light as a function of the emission, and the function of the fit line is $E_m = 1.00E_x + dE$ ($R^2 = 0.9983$) with $\Delta E = 1.1$ eV. (b) A schematic illustration of various typical electronic transitions processes of GQDs (reprinted with permission from ref. 51. Copyright 2011). (c) The up-conversion PL properties of GQDs *via* solvothermal method. (Reprinted with permission from ref. 85. Copyright 2012). (d) Upconverted PL spectra of the ultrasonically synthesized GQDs at different excitation wavelengths (reprinted with permission from ref. 12. Copyright 2012).

3.3 Electrochemiluminescence (ECL)

Electrochemiluminescence (ECL) not only exhibits the advantages of chemiluminescence detection, like the high sensitivity and wide concentration working range, but also assures specific advantages, such as an enhanced selectivity, extended analytical application and improved detection spatial resolution.[99] Since the discovering of the ECL from silicon QDs by Ding *et al.* in 2002,[100] more and more quantum dots, such as CdSe,[101] CdTe (ref. 102) and CDs,[37,43,103] were reported to possess ECL properties and found their analytical applications.

ECL was also observed from GQDs prepared *via* a microwave-assisted approach.[6] As shown in Fig. 18a, when the potential was cycled negatively between 0 and −1.6 V in the presence of 0.1 M $K_2S_2O_8$ as co-reactant, GQDs showed an intense ECL emission at −1.45 V with an onset potential at about −0.9 V, which was about 9 times higher than background signal. No obvious ECL was observed in the absence of $K_2S_2O_8$, indicating the important role of $K_2S_2O_8$ as co-reactant. The mechanism was described in Fig. 18b. Firstly, strongly oxidizing $SO_4^{\cdot-}$ radicals and $GQDs^{\cdot-}$ radicals were produced by electrochemical reduction of $S_2O_8^{2-}$ and GQDs, respectively, Then, $SO_4^{\cdot-}$ radicals could react with $GQDs^{\cdot-}$ *via* electron-transfer annihilation, producing an excited state (GQDs*) that finally emitted light. An attractive merit of gGQDs in ECL study is the well-defined ECL peak at relatively positive potential in comparison with previously reported CDs.[37,43] Besides, the ECL spectrum of GQDs with the maximum wavelength at 512 nm, which was slightly red-shifted (12 nm) in comparison with the PL spectrum, indicating the GQDs had negligible surface defect.

3.4 Cytotoxicity

The toxicity of GQDs is a natural concern because of their potential for bio-applications. The cytotoxicity of GQDs has been evaluated by various research groups, revealing that GQDs appear to have low toxicity.[13,16,17,52,54,74,77] Zhu *et al.* performed cell viability tests on MG-63 (Human osteosarcoma) cells using methylthiazolyldiphenyl-tetrazolium bromide (MTT) assay.[16] Adding up to 400 μg of GQDs to 150 mL of culture medium (10^4 cells) did not weaken the cell activity significantly (Fig. 19a), suggesting that GQDs posed low toxicity effects and could be used in bioimaging and other biomedical applications with high concentration. MTT assays have also been performed by Zhang *et al.* with three different kinds of stem cells, neurospheres cells (NSCs), pancreas progenitor cells (PPCs) and cardiac progenitor cells (CPCs).[54] Average cell viability of NSCs and CPCs was above 80% after 3 days culturing with GQDs at the GQDs concentration of 100 mg mL^{-1}, and was about 65% for PPCs, while all the cells could be clearly observed after incubation in 25 mg mL^{-1} GQDs solution. Besides, MC3T3 cells,[13] human breast cancer MCF-7 cells,[17] HeLa cells[74] and two different human breast cancer cell lines MDA-MB-231 and T47D[52] have been adopted to evaluate the cytotoxicity of GQDs. All these studies suggest that GQDs have low cytotoxicity and are greatly promising for bio-applications, such as *in vitro* and *in vivo* imaging studies.

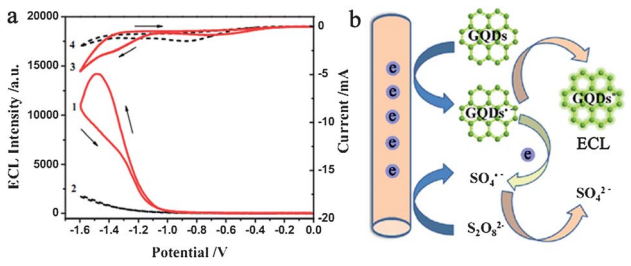

Fig. 18 (a) ECL-potential curves and cyclic voltammograms (CVs) of the gGQDs (1 and 3) and background (2 and 4) with concentration of 20 ppm in 0.05 M Tris–HCl (pH 7.4) buffer solution containing 0.1 M $K_2S_2O_8$. Scan rate: 100 mV s^{-1}. (b) Schematic illustration of the ECL mechanism of GQDs (reprinted with permission from ref. 6. Copyright 2012).

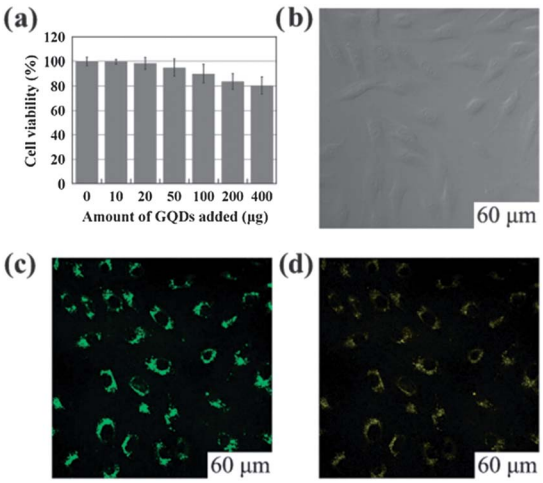

Fig. 19 (a) Effect of GQDs on MG-63 cells viability. (b), (c) and (d) are washed cells imaged under bright field, 405 nm and 488 nm excitations, respectively (reprinted with permission from ref. 16. Copyright 2011).

3.5 Bandgap engineering

GQDs feature tunable bandgap due to their pronounced quantum confinement and edge effects. The bandgap in graphene-based materials can be tuned from 0 eV to that of benzene by changing size and/or surface chemistry, making it a rising carbon-based fluorescent material.[58] Li *et al.* reported that the band gaps and redox potentials of GQDs could be independently controlled, the former by size and the latter by functionalization.[73] Based on the two major strategies, currently, increasing efforts have been made to customize their optical properties, among which the tunability based on the variation of size has already been discussed in the above section, Size dependence. Other strategies can be classified in to three main groups: tuning oxidation degree, surface functionalization, and chemical doping, which are discussed in detail as below.

3.5.1 Tuning oxidation degree. As discussed above, the oxygen-containing functional groups on GQDs can lead to radiative recombination of localized electron–hole pairs and surface emissive traps. And the variation of the degree of oxidation (or reduction) can induce the alteration of localized

sp^2 clusters and structural defects, thus changing the PL.[19,57] Li *et al.* prepared greenish-yellow luminescent GQDs (gGQDs) *via* a microwave-assisted method with QY of 11.7%, and they found that when the gGQDs are further reduced with $NaBH_4$, bright blue luminescent GQDs (bGQDs) are obtained with a QY as high as 22.9%.[6] The dimensions and heights of gGQDs and bGQDs were identical, indicating that the PL blue-shift of bGQDs could be attributed to their structural change after reduction rather than size effect. Zhu *et al.* got three batches of solvothermally prepared GQDs utilizing gradient elution.[85] Though GQDs in three batches possessed similar sizes and heights (3–5 nm, 0.95 nm, respectively), they had tuned optical properties due to the increasing degree of surface oxidation from Batch 1–3, see Fig. 20a. The higher degree of surface oxidation could result in more surface defects, leading to the red-shifted emission. The PL quantum yields were measured to be 4.1, 9.9 and 12.2%, respectively. Zhu *et al.* further reduced the green luminescent GQDs by to $NaBH_4$ to obtain blue luminescent rGQDs, with QY increasing from 5.9% to 12.1%.[13] They claimed that the carbonyl, epoxy and amido moieties were changed into –OH groups in rGQDs upon reduction, which suppressed non-radiative process and further enhanced integrity of π conjugated system (also reduce the defects).

3.5.2 Surface functionalization. Chemical modifications using molecules with strong electron-donating or -accepting ability could also result in appreciable impact on electronic characteristics of grapheme. Li *et al.* demonstrated that, the electron-donating groups generally raised the HOMO levels, and electron-withdrawing groups lowered the LUMO levels.[73]

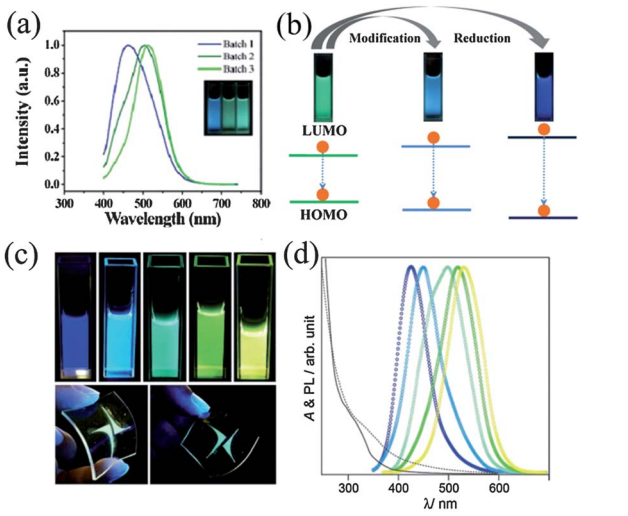

Fig. 20 (a) PL spectra of Batch 1–3 at 380 nm excitation (inset: photograph of three components taken under UV light (365 nm)) (reprinted with permission from ref. 85. Copyright 2012). (b) Scheme of bandgap changing of GQDs, m-GQDs and r-GQDs (reprinted with permission from ref. 13. Copyright 2012). (c) Emission images of af-GQDs dispersed in water (upper) and af-GQDs@polymer hybrids (bottom) under irradiation from a 365 nm UV lamp. The af-GQDs in the upper images were prepared under the following conditions: 150 °C, 120 °C, 70 °C, 90 °C, and 90 °C in 2× conc. ammonia solution, respectively from the left. (d) PL spectra corresponding to the af-GQDs shown in the upper image of panel (c) (reprinted with permission from ref. 58. Copyright 2012).

Apart from the rGQDs, Zhu *et al.* also prepared blue luminescent mGQDs from green luminescent GQDs *via* chemical modification with alkylamines (Fig. 20b).[13] Upon reaction, previously existing –COOH and epoxy groups in GQDs that always induced non-radiative recombination of localized electron–hole pairs and hold back the intrinsic state emission,[23] were replaced by –CONHR and –CNHR. The newly appeared groups could suppress the non-radiative process, thus enhancing the intrinsic state emission. The QY of mGQDs was 6.5%, higher than that of GQDs (5.9%). Tetsuka *et al.* prepared amino-functionalized GQDs (af-GQDs) *via* amino-hydrothermal method (see Fig. 3) with high efficiency and clear multiple colors under a single-wavelength UV excitation (Fig. 20c and d).[58] The degree of amine functionalization, which controlled the PL color, could be controlled simply by changing the initial concentration of ammonia and the temperature of the amino-hydrothermal treatment. The resonance feature between the delocalized π orbital and the molecular orbital in the $–NH_2$ amino group was the origin of both the optical tunability and the high QY (over 40%).

Zhang *et al.* reported that, when the electrochemically synthesized GQDs were reduced with hydrazine hydrate at room temperature, the hydrazide groups were formed on the GQD edges by the reaction of hydrazine with the peripheral carboxylic acid groups.[54] The strong yellow luminescence from the GQDs was emitted by a high concentration of modified hydrazide groups after absorption through the graphene π–π* and n–π* transitions. When the reducing agent hydrazine hydrate was changed to $NaBH_4$ under otherwise the same conditions, no yellow but weak blue light could be observed.

3.5.3 Chemical doping. Doping carbon nanomaterials with heteroatoms can effectively tune their intrinsic properties, including electronic properties, surface and local chemical reactivity.[68,104,105] Especially, the N atom has been widely used for chemical doping of carbon nanomaterials, such as N-doped carbon nanotubes (N-CNTs),[106] and N-doped graphene.[96,107] N-doped GQDs (N-GQDs) have also been reported by several groups. In view of the remarkable quantum-confinement and edge effects of GQDs, doping GQDs with chemically bonded N atoms could drastically alter their electronic characteristics and offer more active sites, thus producing new phenomena and unique properties.[68] The electrochemically prepared N-GQDs were firstly reported by Qu *et al.*, using N-containing tetrabutylammonium perchlorate (TBAP) in acetontrile as the electrolyte to introduce N atoms into the resultant GQDs *in situ*.[68] The high-resolution N 1s spectrum of the N-GQDs with N/C atomic ratio of *ca.* 4.3% revealed the presence of both pyridine-like and pyrrolic N atoms. Unlike their green luminescent N-free counterparts, N-GQDs emitted blue luminescence with QY as a result of the relatively strong electron affinity (electron-withdrawing ability) of N atoms in the N-GQDs. N-GQDs also possessed an electrocatalytic activity for the oxygen reduction reaction (ORR) in an alkaline medium, comparable to that of a commercially available Pt/C catalyst. Tang *et al.* developed a hydrothermal approach for the synthesis of N-GQDs by cutting N-doped graphene.[105] The N-GQDs obtained had N/C atomic ratio of *ca.* 5.6% and diameter of 1–7 nm. The N-GQDs exhibited bright

blue PL performance and excellent upconversion properties. N-GQDs with higher N/C atomic ratio (17.88%) have further been prepared by Hu *et al.* through hydrothermal treatment of GO in the present of ammonia, where both pyridine-like and pyrrolic N atoms were present.[74] The as-prepared N-GQDs were highly blue-luminescent with a maximum QY as high as 24.6%.

3.6 Assembly of GQDs

The assembly of QDs in a geometrically well-defined fashion opens up opportunities to control over the optical and electronic coupling between the individual QD units, thus providing the possibility to get access to the full potential of assembled QDs by virtue of the their collective properties.[108,109] Li *et al.* showed assemblies of colloidal GQDs over large areas on polar surfaces and the control of their orientations.[110] The orientations of the GQDs could be determined, either in- or out-of-plane (*i.e.*, "face-on" and "edge-on", respectively) with the substrate, by chemical functionalization that introduced orientation-dependent interactions between GQDs and the surfaces. The orientation of the GQDs is controlled by built-in chemical information that guided the assembly. Qu *et al.* developed a well-organized assembly of functional GQDs into 1D nanotube (NT) arrays by electrophoresis deposition within a nanoporous AAO template.[108] The hierarchically porous 1D nanotube structure of 0D GQDs could ensure more efficient charge transfer between the target molecules and the GQDs and thus produced much stronger SERS effect, exceeding that on the flat graphene sheets. Consequently, this 1D nanotubes of 0D GQDs demonstrated their remarkable potential as a new metal-free platform for efficient surface-enhanced Raman scattering (SERS) applications. Later on, the same group prepared GQDs microspheres (GQDSs) by assembly of GQDs *via* a water-in-oil (W/O) emulsion technique without the addition of any surfactants.[109]

In addition, Li *et al.* also used colloidal GQDs to study metal–carbon interaction.[111] Pd nanoparticles were synthesized in the presence of the GQDs and subsequently stabilized by them to prevent their aggregation. The Pd particles had sizes near 1 nm and consisted of ~34 atoms, while the GQDs had a dimension of ~2.5 nm on the longest edge, large enough to support Pd particles. The nanoparticles significantly altered the graphene conjugation, indicating the covalent nature of their interaction. Son *et al.* prepared emissive ZnO–graphene quasi-core–shell QDs consisting of a ZnO core wrapped in a shell of single-layer graphene and adopted them to make a white-light-emitting diode.[112]

4 Applications

4.1 Bioimaging

Optical properties are the key for GQDs to be put into practical use. The bright PL and established low cytotoxicity render GQDs applicable in biological applications such as bioimaging. Peng *et al.* selected the green luminescent GQDs to incubate with human breast cancer cell lines T47D with the nucleus stained with DAPI (blue color).[52] Fig. 21 showed the images of T47D cells treated with green GQDs for 4 h incubation time, which clearly

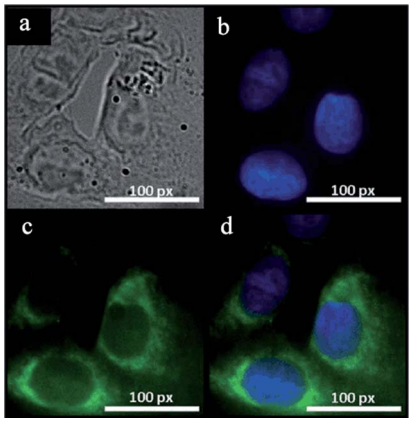

Fig. 21 Fluorescent images of human breast cancer cell T47D after incubation with green GQDs for 4 h. (a) Phase contrast picture of T47D cells. (b) Individual nucleus stained blue with DAPI. (c) Agglomerated green GQDs surrounding each nucleus. (d) The overlay high contrast image of nucleolus stained with blue DAPI and GQDs (green) staining (reprinted with permission from ref. 52. Copyright 2012).

visualized the phase contrast image of T47D cells with nucleus stained with blue DAPI, agglomerated high contrast fluorescent image of green GQDs around each nucleus and overlay image of cell with phase contrast, DAPI and green GQDs. These obtained images indicated that GQDs can be used in high contrast bioimaging. The excitation-dependent PL behavior of the GQDs can give rise to numerous visible results. Zhu *et al.* cultured MG-63 cells with solvothermally prepared GQDs and showed the two-color imaging by using different excitation wavelength, as shown in Fig. 19c–d.[16] Dong *et al.* treated human breast cancer MCF-7 cells with green GQDs prepared *via* acidic oxidation for 4 h, and a bright green colour could be seen when imaged on the confocal laser scanning micro-scope with excitation at 488 nm.[17] The section analysis indicated that GQDs were able to label the cell membrane, the cytoplasm, and the nucleus simultaneously. That is the first time for luminescent carbon nanomaterials to label the cell nucleus. Besides, HeLa cells have also been adopted to incubate with green luminescent GQDs by several groups.[62,74,77]

Zhang *et al.* applied GQDs in stem cell labeling, which posed a considerable challenge, as currently no technique was available for labeling stem cells directly and efficiently because of the particularity of stem cells.[54] Three different kinds of stem cells, neurospheres cells (NSCs), pancreas progenitor cells (PPCs) and cardiac progenitor cells (CPCs) were selected and incubated with GQDs at a final concentration of 25 mg mL^{-1} for 24 h at 37 °C. Fig. 22a and b show the confocal fluorescent image of the GQDs-stained NSCs stem cells with an excitation wavelength of 405 nm. The morphology of the cells can be clearly discerned with the internalized GQDs. The confocal section images showed that GQDs easily penetrated into the stem cells but did not enter the nuclei, suggesting that genetic disruptions of the living stem cells by the GQDs didn't happen. They also found that GQDs showed high photostability in the cells and little cytotoxicity according to the MTT assays (Fig. 22c). However, when the stem cells were incubated with semiconductor quantum dots (QDs), 5 nm CdS nanoparticle without surface

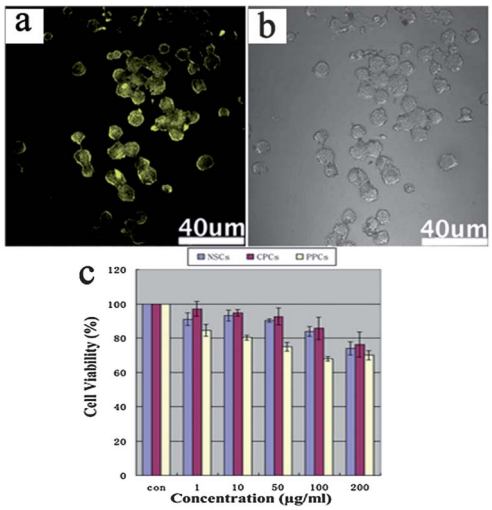

Fig. 22 Confocal fluorescence microscopy images of stem cells of NSCs (a) and corresponding images under bright field (b). (c) Cell viability for the stem cells of NSCs, CPCs and PPCs as a function of the added GQDs concentration (reprinted with permission from ref. 54. Copyright 2012).

modification, the stem cells died owing to the cytotoxicity of Cd^{2+}. Therefore, the GQDs have a distinct advantage in terms of their biocompatibility, low cytotoxicity and high photostability.

The above reports used downconversion PL induced by one-photon UV or blue excitations which are harmful to living cells or biosystems. The upconversion PL of GQDs exhibited the advantage in harvesting near-IR light using multi-photon excitation. Zhu *et al.* have observed bright green or blue areas inside the GQDs-stained MC3T3 cells under near-IR excitation (808 nm), indicating successful translocation of GQDs through cell membrane.[13] Furthermore, no obvious reduction in PL brightness was observed under continuous excitation over 20 min, indicating high photostability of GQDs.

4.2 Drug delivery

Zhu *et al.* fabricated multifunctional core–shell structure capsules composed of olive oil, dual-layer porous TiO_2 shell, Fe_3O_4 and GQDs.[113] The olive oil acted as the reservoir of oil-soluble drug. The TiO_2 shell suppressed the initial burst release of the paclitaxel. The Fe_3O_4 and GQDs inside the oil core functioned successfully for magnetic targeting and fluorescence imaging respectively. Furthermore, paclitaxel in capsules was trigger released by ultrasound stimulation, and the release profile could be controlled by the length of repeatable ultrasound time. The results indicated that these core–shell capsules were expected to play a significant role in the development of water-insoluble drug's controlled-release and delivery. Nanographene (NGO) has also been applied to drug delivery by Dai *et al.* Insoluble aromatic drug SN38, a potent topoisomerase I inhibitor, was attached onto PEGylated NGO (NGO-PEG) *via* simple adsorption.[114] The resultant NGO-PEG-SN38 complexes were water soluble at concentrations up to ~1 mg mL^{-1}, and afforded highly potent cancer cell killing *in vitro* with IC_{50} values of ~6 nM for HCT-116 cells, which was ~1000-fold more potent than CPT-11 and similar to that of free SN38 dissolved in DMSO. They also found that simple physisorption *via* π–π stacking could be used for loading doxorubicin, a widely used cancer drug onto NGO functionalized with antibody for selective killing of cancer cells *in vitro*.[115]

4.3 DNA cleavage system

The exploration of efficient DNA intercalators is essential for understanding DNA scission, repair, and signal transduction. Zhou *et al.* showed another interesting application of GQDs in DNA cleavage system.[9] They found that, by using GQDs and Cu^{2+}, about 90% supercoiled DNA was converted into nicked DNA, while only about 59% supercoiled DNA was cleaved with the same amount of large size GO and Cu^{2+}. They speculated that the as-prepared GQDs sheets with smaller lateral size will be a better intercalator to DNA molecules than micrometer-sized GO sheets. Therefore, under the same condition, GQDs had higher efficiency than GO for DNA cleavage. This result can open further potential applications of GQDs in biological and medical research.

4.4 Sensors

4.4.1 PL sensors. Based on the PL of GQDs, various sensors have been fabricated recently with either signal-off or signal-on processes. Wang *et al.* firstly reported that GQDs could be used for Fe^{3+} detection on the basis of the selective fluorescence quenching effect to Fe^{3+}.[116] Taking into account the special coordinate interaction between Fe^{3+} ions and phenolic hydroxyl group which was responsible for the PL of GQDs, the photoluminescence of GQDs could be greatly affected by Fe^{3+} ions. Fig. 23a shows the fluorescence change GQDs with and without addition of 80 ppm Fe^{3+} ions, showing that the fluorescence of GQDs in the presence of Fe^{3+} ions was almost completely quenched, while other metal ions (Zn^{2+}, Cd^{2+}, Ca^{2+}, Mg^{2+}, Pb^{2+}, Fe^{2+}, Cu^{2+}, $Ru^{3+}$and Fe^{3+}) at the same concentration had much weaker influence on the fluorescence of GQDs. In the range of 0.8–8 ppm of Fe^{3+} ions, fluorescent quenching value was detectable and presented an almost linear relationship (Fig. 23b). The detection limit of Fe^{3+} ions for 0.12 mg mL^{-1} GQDs dispersion was calculated to be around 1 ppm. Fan *et al.* reported that GQDs could serve as an effective and simple fluorescent sensing platform for ultrasensitive detection of 2,4,6-trinitrotoluene (TNT) in solution by fluorescence resonance energy transfer (FRET) quenching.[96] The TNT species could specifically attached onto the fluorescent GQDs by the π–π stacking interaction between GQDs and aromatic rings. And the attached TNT could strongly suppress the fluorescence emission by the FRET from GQDs donor to the irradiative TNT acceptor through intermolecular polar–polar interactions at spatial proximity. 1 mL of unmodified GQDs could sensitively detect down to ~0.495 ppm (2.2 mM) TNT.

In addition, PL biosensors have been fabricated for biomaterials detection. Yang *et al.* found that the PL intensity of GQDs decreased with the increasing concentration of pyrocatechol.[69] They stated that the oxygen-containing groups in GQDs enabled noncovalent interaction between GQDs and pyrocatechol

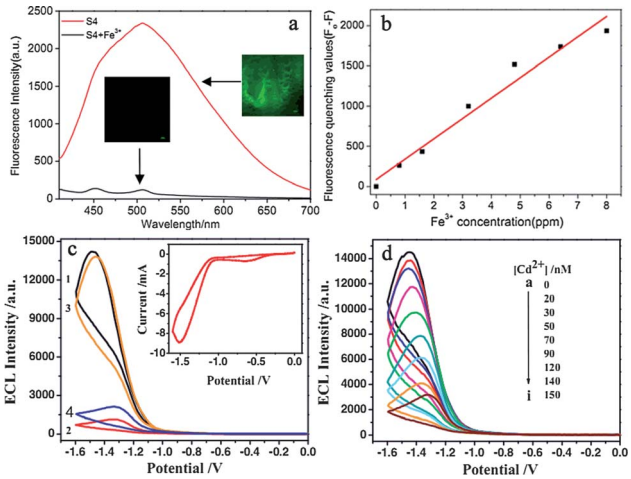

Fig. 23 (a) Fluorescence spectra of sample S4 with and without addition of Fe^{3+} ions (insets: right one is the fluorescence imaging of S4 without addition of Fe^{3+} ions. Left one is the fluorescence imaging of S4 with addition of 80 ppm Fe^{3+} ions). (b) The curve of the fluorescence quenching values ($F_0 - F$) *vs.* Fe^{3+} ion concentration in the range from 0.8 ppm to 8 ppm (reprinted with permission from ref. 106. Copyright 2012). (c) ECL–potential curves of the gGQDs (1), the gGQDs with the addition of 20 μM Cd^{2+} (2), the gGQDs with the successive addition of 20 μM Cd^{2+}, 40 μM EDTA (3), or 1 mM Cys (4) in 0.05 M, pH 7.4 TBS with 0.1 M $K_2S_2O_8$. Inset: CV corresponds to (2). (d) ECL–potential curves of gGQDs in the presence of (a–i) 0, 20, 30, 50, 70, 90, 120, 140 and 150 nM Cd^{2+}. The electrolyte is 0.05 M, pH 7.4 TBS with 0.1 M $K_2S_2O_8$ and 1 mM Cys (reprinted with permission from ref. 6. Copyright 2012).

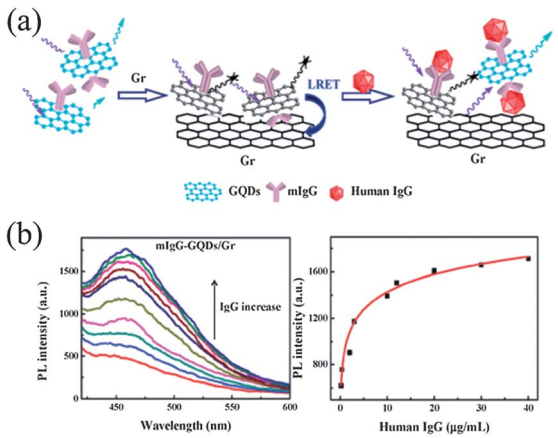

Fig. 24 (a) Schematic illustration of a universal immunosensing strategy based on regulation of the interaction between Gr and GQDs. (b) Changes in the PL spectra of mIgG-GQDs upon increasing the concentration of human IgG (left), and the corresponding plot of the PL intensity against the concentration of human IgG (reprinted with permission from ref. 15. Copyright 2012).

through electrostatic interaction, π–π stacking or hydrogen bonding, leading to the energy transfer and further the PL quenching of GQDs. The plot of the fluorescence intensity ratio (F_0/F) *vs* the negative logarithm value of pyrocatechol concentration showed the spectral response range from 5.00×10^{-3} mol L^{-1} to 1.0×10^{-7} mol L^{-1}. In addition, Zhao *et al.* provided a novel and versatile signalling transduction strategy through luminescence resonance energy transfer (LRET) between graphene (Gr) and GQDs for the sensitive detection of human immunoglobulin G (IgG).[15] As shown in Fig. 24a, Gr as an acceptor and mouse anti-IgG (mIgG, antibody)-conjugated GQDs as donors were chosen to fabricate a LRET immunosensor for detecting IgG. When adding Gr to the mIgG-GQDs solution, the π–π stacking interaction between Gr and GQDs would bring Gr and GQDs into LRET proximity, thus facilitating the luminescence quenching of GQDs. However, the addition of HIgG would effectively increase the distance between mIgG-GQDs and Gr surface due to the specific antibody–antigen interaction, thus hindering the LRET process and then producing a restoration of luminescence. The overall luminescence response depended on the amount of IgG in the samples, thus providing an effective basis for quantitative determination of IgG (see Fig. 24b). The PL intensity increased with increasing concentration of human IgG in the range from 0.2 to 12 μg mL^{-1} and reached a plateau after the human IgG concentration exceeded 20 μg mL^{-1}.

4.4.2 ECL sensor. On the basis of the intense ECL of GQDs discussed above, Li *et al.* applied them in the determination of Cd^{2+}.[6] They found that six kinds of ions, including Ni^{2+}, Pb^{2+}, Cu^{2+}, Co^{2+}, Fe^{2+} and Cd^{2+} could quench the ECL, when the metal ions (20 μM) were added into the pH 7.4 TBS (0.05 M) with 0.1 M $K_2S_2O_8$ and 20 ppm GQDs. The ECL quenching could be induced by the interaction between metal ions and GQDs. The obtained GQDs were covalently decorated with oxygen-containing functional groups, such as hydroxyl and carboxyl groups, as well as doped nitrogen, which had complexation ability with metal ions. Therefore, they served as effective coordination groups for metal ions, forming a Cd^{2+}-GQDs complex and thereby induced the aggregation of GQDs, leading to the decrease of corresponding ECL emission. Furthermore, it was found that when a certain amount of ethylenediaminetetraacetic acid (EDTA) was added, the quenched ECL could be almost completely recovered (Fig. 23c, grey line) as EDTA could prevail over GQDs and resulted in decomplexation of metal ion-GQDs complex, giving rise to the recovery of ECL. Another interesting phenomenon was observed that the addition of cysteine (Cys) could recover the quenched ECL induced by all the metal ions (20 μM) except Cd^{2+}, which quenched the GQDs ECL by 85% even in the presence of 1 mM Cys (Fig. 23c). Thus Cys could act as effective masking agent for the determination of Cd^{2+} with acceptable selectivity. As shown in Fig. 23d, the ECL intensity of GQDs was gradually decreased with increasing Cd^{2+} concentration in the presence of 1 mM Cys. The proposed sensor shows a linear relationship between the Cd^{2+} concentration with ECL intensity decrease over the range from 20 nM to 150 nM ($R = 0.998$) with a detection limit of 13 nM at signal-to-noise of 3. This novel ECL sensor for Cd^{2+} is comparable with other methods such as colorimetric and fluorescence sensors.

4.4.3 Electrochemical sensor. GQDs possess some of the excellent properties of graphene, such as good electron mobility and chemical stability. Zhao *et al.* had designed a simple but smart platform to fabricate electrochemical biosensors by using GQDs modified pyrolytic graphite electrode coupled with specific sequence ssDNA molecules as probes.[117] GQDs were

readily modified onto the surface of pyrolytic graphite (PG) electrode, and then the probe ssDNA (ssDNA-1) could be easily immobilized due to the interaction between the nucleobases and graphene. The immobilized ssDNA would inhibit the electron transfer between the electro-active species $[Fe(CN)_6]^{3-/4-}$ and the electrode because of the electrostatic repulsion, leading to a drastic decrease of the electrochemical signal. However, when the target molecules such as target ssDNA (ssDNA-2) or target protein also existed in the test solution, the probe ssDNA would bind with the target instead of graphene if the sequence of the probe ssDNA was designed as complementary to the ssDNA-2 or as the aptamer of the target protein. Thus, the electrostatic repulsion to the electro-active species $[Fe(CN)_6]^{3-/4-}$ resulted from the immobilized ssDNA would be removed, thus increasing the obtained peak currents. No label was needed for the probe DNA in this detection, which made the detection much more simple and cheap to be performed.

Razmi and Mohammad-Rezaei developed a biosensor by immobilizing glucose oxidase (GOx) on GQDs modified carbon ceramic electrode (CCE), which responded efficiently to glucose presence over the concentration range 5–1270 μM with the detection limit 1.73 μM ($S/N = 3$).[14] High performance of the biosensor is attributed to the large surface-to-volume ratio, excellent biocompatibility of GQD, and the abundance of hydrophilic edges as well as hydrophobic plane in GQD which enhances the enzyme absorption on the electrode surface.

4.5 Photocatalyst

The TiO_2 semiconductor is the most widely used photocatalyst due to the long-term thermodynamic stability, strong oxidizing power, and relative nontoxicity. The photocatalytic oxidation process is initiated through the photogeneration of electron/hole pairs under UV light, the wavelength of which is lower than that corresponding to the band-gap energy of TiO_2.[118] Therefore, the activity of TiO_2 is limited under the visible light irradiation and there is a great need to extend the light absorption to the visible light region. Developing composite materials such as CNTs/TiO_2 (ref. 119) and graphene/TiO_2 (ref. 120) nanocomposites, have been studied extensively for improving the photocatalytic activity of TiO_2.

Zhuo *et al.* designed photocatalysts (rutile TiO_2/GQD and anatase TiO_2/GQD complex systems) to harness the visible spectrum of sunlight, based on the upconversion luminescence properties of GQDs.[12] Their photocatalytic ability was determined by degradation of methylene blue (MB) under Xe lamp irradiation (with 420 nm cutoff filter). As can be seen in Fig. 25a, the photodegradation efficiency is up to 97% in 60 min with the rutile TiO_2/GQD complex and 31% with anatase TiO_2/GQD complex acting as photocatalysts. The reason might be explained as in Fig. 25b. Under visible light ($\lambda > 420$ nm) irradiation, the upconverted PL peak of GQDs was located at *ca.* 407 nm (3.05 eV). This energy was larger than the band gap of rutile TiO_2 3.0 eV (414 nm), yet smaller than that of anatase TiO_2 3.2 eV (388 nm). Hence the photocatalytic ability of rutile TiO_2/GQD was much superior to that of the anatase TiO_2/GQD complex. Contrast experiments were carried out using only pure

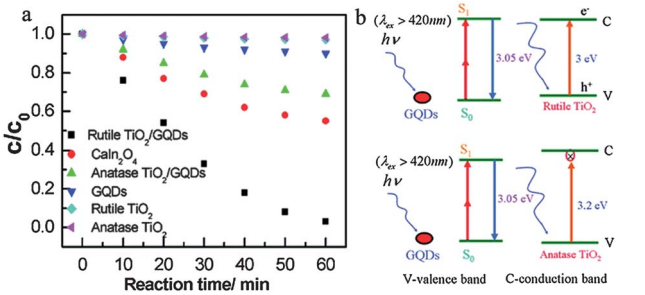

Fig. 25 (a) Relationship between MB concentration and reaction time for different catalysts: rutile TiO_2/GQDs, $CaIn_2O_4$, anatase TiO_2/GQDs, GQDs, rutile TiO_2 NPs, and anatase TiO_2 NPs. (b) Schematic of photocatalytic process for (a) rutile TiO_2/GQD and (b) anatase TiO_2/GQD under visible light ($\lambda > 420$ nm) irradiation (reprinted with permission from ref. 12. Copyright 2012).

rutile TiO_2 (50 mg), pure anatase TiO_2 (50 mg), pure GQDs (5 mL) and $CaIn_2O_4$ as photocatalysts. The result indicated that the excellent photocatalytic activities of TiO_2/GQD should be attributed to the interaction between GQDs and TiO_2.

4.6 Energy-related applications

Organic photovoltaic (OPV) devices have attracted increasing attention since the report of two-layer organic photovoltaic cell by Tang[121] Usually, the OPV cells are those with bulk heterojunction (BHJ) architecture based on soluble poly(3-hexylthiophene) (P3HT) and poly(3-octylthiophene) (P3OT) as the donor and PCBM as the acceptor.[122,123] Recently, graphene was applied as the acceptor[124,125] and could also replace the common ITO as the transparent electrode[120,126,127] due to its remarkable electronic and mechanical properties. However, graphene sheets have extremely poor solubility and have a strong tendency to aggregate into graphite. The properties of large solubility and tunable band gap make GQDs very attractive for photovoltaic applications.

The graphene quantum dot 1 discussed above in Fig. 10a, was used as a sensitizer for dye-sensitized solar cells by Yan *et al.*[8] Quantum dot 1 absorbed a wide spectrum of light from visible to near IR with an absorbance maximum at 591 nm. According to the calculated HOMO and LUMO energy levels of 1, band levels of TiO_2 and reduction potential of I_3^-/I^-, it was possible for 1 to inject an electron to TiO_2 and then get regenerated by accepting an electron from I^- upon photoexcitation. Thus graphene quantum dot 1 replaced traditionally used ruthenium complexes as the sensitizer in nanocrystalline TiO_2 solar cells. Similarly, Dutta *et al.* reported a combination GQDs with ZnO NWs to demonstrate their potential as a solar harvesting material in photovoltaic cells.[128] ZnO has been widely used in solar cells as electrode buffer layers or transparent electrodes.[129–131] Notably, when combined with GQDs, charge-transfer process took place at the interface between GQDs and ZnO NWs. The photovoltaic cell comprised of these GQDs showed a high open circuit voltage (V_{OC}) of ~0.8 V and the IQE reached a value of 87% at the absorption maximum (Fig. 26a). A clear photovoltaic effect was observed from the *I–V* curve (Fig. 26b) of the device made with the composite, indicating and

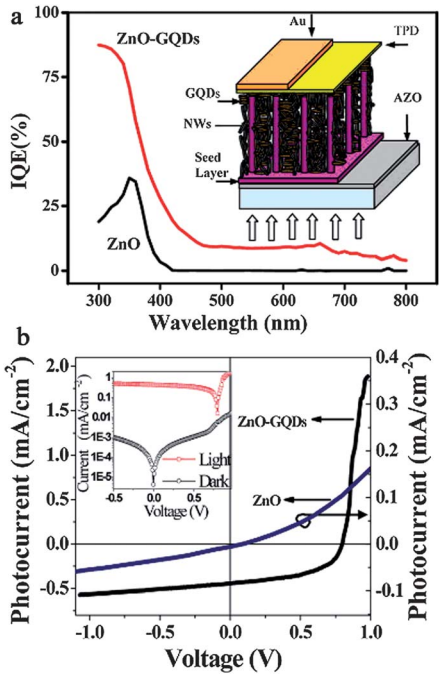

Fig. 26 (a) IQE of the samples. The inset shows the schematic model of the device. (b) Solar cell *I–V* characteristics under white light illumination. The inset shows the logarithmic plot of dark and photo current of the GQDs-ZnO cell (reprinted with permission from ref. 128. Copyright 2012).

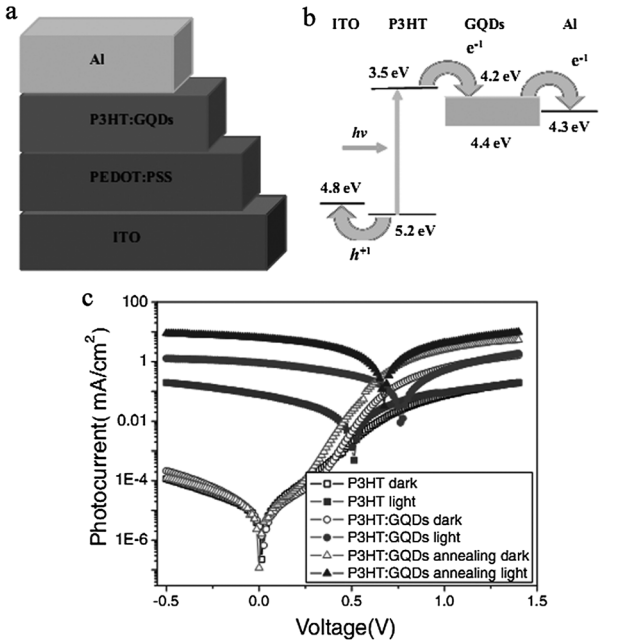

Fig. 27 Schematic (a) and energy band (b) diagrams of the ITO/PEDOT:PSS/P3HT:GQDs/Al device. (c) *J–V* characteristic curves for the ITO/PEDOT:PSS/P3HT/Al, ITO/PEDOT:PSS/P3HT:GQDs/Al and ITO/PEDOT:PSS/P3HT:GQDs/Al devices after annealing at 140 °C for 10 min, single log scale (reprinted with permission from ref. 53. Copyright 2011).

confirming that there was an electron injection into the NWs from the excited GQDs. Though the efficiency of the present GQDs-sensitized solar cell was quite low, it might be improved when improving the hole conduction by regulating the thickness of GQDs layer and spacing between NWs.

Li *et al.* applied GQDs as novel electron acceptor in a P3HT-based solar cell.[53] As shown schematically in Fig. 27a, polymer photovoltaic cells with the structure of ITO/PEDOT:PSS/P3HT:GQDs/Al were fabricated, where ITO, PEDOT, PSS and P3HT stranded for indium tin oxide, poly(3,4-ethylenedioxythiophene), poly(styrenesulfonate) and poly(3-hexylthiophene), respectively. Fig. 27b gives the energy level diagram for the GQD-based photovoltaic cells where the LUMO level of GQDs is estimated to be in the range of 4.2–4.4 eV by electrochemical methods. Compared with the P3HT device, the performance of GQD-based devices, in terms of such quantities as I_{sc}, V_{oc}, FF and PCE, was enhanced overall due to the contribution of GQDs in this device (Fig. 27c). In the P3HT:GQDs composite device, the GQDs provides a large surface area for the formation of p–n interfaces and carrier transporting pathways. Although without device optimization in this primary study, a power conversion efficiency of 1.28% was achieved.

The O-containing groups on the surface of GQDs make them an interesting class of materials to combine with other active components for complex functions. Gupta *et al.* functionalized GQDs with aniline (ANI) for solar cell applications and with methylene blue (MB) dye for organic light emitting diode (OLED) applications.[18] The formed OPV device and OLED device have the structure of ITO/PEDOT:PSS/P3HT:ANI-GQDs/LiF/Al and ITO/PEDOT:PSS/MEH-PPV:MB-GQDs/LiF/Al, respectively. The GQDs dispersed in conjugated polymers showed enhanced OPV and OLED characteristics as compared to GSs due to improved morphological and optical characteristics.

5 Conclusions and future perspectives

In this review, GQDs have been comprehensively introduced from the aspects of synthetic approaches, optical properties to present applications. Not surprisingly, based on their pronounced quantum confinement and edge effects, excellent chemical stability, biocompatibility/nontoxicity, GQDs have ignited tremendous and increasing research interest. However, the research on GQDs is still at its early stage, and most of the references concerning GQDs in this review appear in the last 3 years. Therefore, on one hand, there is a huge development space for GQDs, and on the other hand, there are still some issues needing to be solved, such as the low product yield and quantum yield, the deficiencies in accurately controlling lateral dimensions as well as surface chemistry, the confusing PL mechanism, the narrow spectral coverage, the lack in tailor-made control of optical properties, *etc.* In view of the development tracks of grapheme, CDs and even semiconductor quantum dots, we speculate the future perspectives on GQDs as follows.

5.1 Unequivocal PL mechanism

Although much efforts has been made, an unequivocal and comprehensive understanding of the optical properties of

GQDs is still absent. GQDs prepared *via* various methods are demonstrated to possess different mechanism, such as size, shape, surface structure, edge effects, *etc.* The GQDs PL is dictated by either the combination or competition between these factors. However, it is quite difficult to point out the detailed PL mechanism in each case. Besides, the current mechanisms are mainly acquired according to the optical behaviours of as-prepared GQDs, leading to the confusing results as each case works in their own ways. Therefore, a full understanding of GQDs optical properties is highly urgent, which will be promising in guiding the synthesis of GQDs with expected properties.

5.2 Advanced synthetic approaches

As shown in Table 1, the product yields of current synthetic approaches are very low (<10% mostly). Therefore, the seeking for high-yield preparation methods is of great importance. The photo-Fenton reaction method showed the highest yield of 45%, nearly 30 times higher than that of solvothermal method. Inspire by this, we can expect that, by using biodegradation or enzyme catalysis in the top-down cutting process, higher product yield may be obtained.

Besides, present top-down methods and bottom-up methods exist their own obstacle respectively. For the former, it is usually difficult to control in terms of size and shape due to the non-selective chemical cutting process.[47] As for stepwise solution chemistry, the rapidly decreasing solubility of graphene with increasing size poses a tremendous challenge to prepare larger GQDs than as-prepared GQDs (<5 nm). Thus, synthesis of high quality GQDs with well controlled size, shape and new solubilization strategy needs to be further explored.

5.3 Expanding the spectral coverage

As shown in Table 1, PL colors of most of the reported GQDs to date are blue to yellow (see Fig. 20c). Although the NIR PL spectrum has been obtained in GQDs synthesized *via* stepwise solution chemistry, its luminescence has not been seen with naked eyes. This narrow spectral coverage limits some applications such as multicolor imaging. Consequently, the explorations in expanding the spectral coverage of GQDs to all visible wavelengths and even NIR will play an important role in the future investigations. This problem may be resolve by the bandgap engineering on GQDs through size control, oxidation degree variation, surface modification and doping. Chu *et al.* reported that the resonant energy transfer between Mn^{2+} and sp^2 clusters of the rGO would enhance the long-wavelength emission.[25] This phenomenon can probably be used in extending GQDs PL spectra to longer wavelength.

5.4 QY improvement

The QYs of GQDs reported so far ranged between 2% and 22.9%, much lower than conventional semiconductor QDs. Therefore the QY improvement is also challenging. Surface passivation could significantly improve the QY of GQDs. Shen *et al.* prepared GQDs-PEG with QY as high as 28.0%, which was two times higher than the GQDs (*ca.* 13.1%).[49] Different passivations should be explored to improve QY, through either two-step or in-situ modifications. It is reported that the QY of CDs prepared from natural gas soot could be dramatically improved from 0.43% to 36.7–60.1% *via* the formation of carbon-metal nanocomposites, with metal ions most likely bound to the peripheral carboxylic moieties by ion exchange or coordination reactions.[98] Such GQDs-metal nanocomposites may also contribute to PL improvement.

Furthermore, with the achievement of uniform size, shape and edge, the multicolor PL and high QY, the GQDs will be more promising in bioimaging, sensors, drug and gene delivery, *etc.* Some new properties, such as magnetism, may also emerge and bring about novel applications.

Acknowledgements

We greatly appreciate the support from National Basic Research Program of China (2011CB933502), National Natural Science Foundation of China (21020102038, 21121091, and 21265014). This work is also supported by Postdoctoral Science Foundation of China (no 2012M521039) and Jiangsu Planned Projects for Postdoctoral Research Funds (1201001B).

Notes and references

1 H. W. Kroto, J. R. Heath, S. C. O'Brien, R. F. Curl and R. E. Smalley, *Nature*, 1985, **318**, 162–163.
2 S. Iijima, *Nature*, 1991, **354**, 56–58.
3 K. S. Novoselov, A. K. Geim, S. V. Morozov, D. Jiang, Y. Zhang, S. V. Dubonos, I. V. Grigorieva and A. A. Firsov, *Science*, 2004, **306**, 666–669.
4 H. Brody, *Nature*, 2012, **483**, S29.
5 L. S. Li and X. Yan, *J. Phys. Chem. Lett.*, 2010, **1**, 2572–2576.
6 L. L. Li, J. Ji, R. Fei, C. Z. Wang, Q. Lu, J. R. Zhang, L. P. Jiang and J. J. Zhu, *Adv. Funct. Mater.*, 2012, **22**, 2971–2979.
7 X. Yan, X. Cui and L. S. Li, *J. Am. Chem. Soc.*, 2010, **132**, 5944–5945.
8 X. Yan, X. Cui, B. Li and L. S. Li, *Nano Lett.*, 2010, **10**, 1869–1873.
9 X. Zhou, Y. Zhang, C. Wang, X. Wu, Y. Yang, B. Zheng, H. Wu, S. Guo and J. Zhang, *ACS Nano*, 2012, **6**, 6592–6599.
10 D. Y. Pan, J. C. Zhang, Z. Li and M. H. Wu, *Adv. Mater.*, 2010, **22**, 734–738.
11 L. Tang, R. Ji, X. Cao, J. Lin, H. Jiang, X. Li, K. S. Teng, C. M. Luk, S. Zeng, J. Hao and S. P. Lau, *ACS Nano*, 2012, **6**, 5102–5110.
12 S. Zhuo, M. Shao and S. T. Lee, *ACS Nano*, 2012, **6**, 1059–1064.
13 S. Zhu, J. Zhang, S. Tang, C. Qiao, L. Wang, H. Wang, X. Liu, B. Li, Y. Li, W. Yu, X. Wang, H. Sun and B. Yang, *Adv. Funct. Mater.*, 2012, **22**, 4732–4740.
14 H. Razmi and R. Mohammad-Rezaei, *Biosens. Bioelectron.*, 2013, **41**, 498–504.
15 H. Zhao, Y. Chang, M. Liu, S. Gao, H. Yu and X. Quan, *Chem. Commun.*, 2013, **49**, 234–236.

16 S. Zhu, J. Zhang, C. Qiao, S. Tang, Y. Li, W. Yuan, B. Li, L. Tian, F. Liu, R. Hu, H. Gao, H. Wei, H. Zhang, H. Sun and B. Yang, *Chem. Commun.*, 2011, **47**, 6858–6860.
17 Y. Dong, C. Chen, X. Zheng, L. Gao, Z. Cui, H. Yang, C. Guo, Y. Chi and C. M. Li, *J. Mater. Chem.*, 2012, **22**, 8764–8766.
18 V. Gupta, N. Chaudhary, R. Srivastava, G. D. Sharma, R. Bhardwaj and S. Chand, *J. Am. Chem. Soc.*, 2011, **133**, 9960–9963.
19 G. Eda, Y. Y. Lin, C. Mattevi, H. Yamaguchi, H. A. Chen, I. S. Chen, C. W. Chen and M. Chhowalla, *Adv. Mater.*, 2010, **22**, 505–509.
20 C. T. Chien, S. S. Li, W. J. Lai, Y. C. Yeh, H. A. Chen, I. S. Chen, L. C. Chen, K. H. Chen, T. Nemoto, S. Isoda, M. Chen, T. Fujita, G. Eda, H. Yamaguchi, M. Chhowalla and C. W. Chen, *Angew. Chem., Int. Ed.*, 2012, **51**, 6662–6666.
21 Z. Luo, P. M. Vora, E. J. Mele, A. T. C. Johnson and J. M. Kikkawa, *Appl. Phys. Lett.*, 2009, **94**, 111909–111903.
22 J. L. Chen and X. P. Yan, *Chem. Commun.*, 2011, **47**, 3135–3137.
23 Q. Mei, K. Zhang, G. Guan, B. Liu, S. Wang and Z. Zhang, *Chem. Commun.*, 2010, **46**, 7319–7321.
24 J. L. Chen and X. P. Yan, *J. Mater. Chem.*, 2010, **20**, 4328–4332.
25 Z. X. Gan, S. J. Xiong, X. L. Wu, C. Y. He, J. C. Shen and P. K. Chu, *Nano Lett.*, 2011, **11**, 3951–3956.
26 G. Xin, H. Wang, N. Kim, W. Hwang, S. M. Cho and H. Chae, *Nanoscale*, 2012, **4**, 405–407.
27 J. Lu, J. X. Yang, J. Wang, A. Lim, S. Wang and K. P. Loh, *ACS Nano*, 2009, **3**, 2367–2375.
28 X. Xu, R. Ray, Y. Gu, H. J. Ploehn, L. Gearheart, K. Raker and W. A. Scrivens, *J. Am. Chem. Soc.*, 2004, **126**, 12736–12737.
29 S. Y. Ju, W. P. Kopcha and F. Papadimitrakopoulos, *Science*, 2009, **323**, 1319–1323.
30 K. Welsher, Z. Liu, S. P. Sherlock, J. T. Robinson, Z. Chen, D. Daranciang and H. Dai, *Nat. Nanotechnol.*, 2009, **4**, 773–780.
31 S. J. Yu, M. W. Kang, H. C. Chang, K. M. Chen and Y. C. Yu, *J. Am. Chem. Soc.*, 2005, **127**, 17604–17605.
32 V. N. Mochalin and Y. Gogotsi, *J. Am. Chem. Soc.*, 2009, **131**, 4594–4595.
33 S. Qu, X. Wang, Q. Lu, X. Liu and L. Wang, *Angew. Chem.*, 2012, **124**, 12381–12384.
34 H. Li, Z. Kang, Y. Liu and S. T. Lee, *J. Mater. Chem.*, 2012, **22**, 24230–24253.
35 S. N. Baker and G. A. Baker, *Angew. Chem., Int. Ed.*, 2010, **49**, 6726–6744.
36 Y. P. Sun, B. Zhou, Y. Lin, W. Wang, K. A. S. Fernando, P. Pathak, M. J. Meziani, B. A. Harruff, X. Wang, H. Wang, P. G. Luo, H. Yang, M. E. Kose, B. Chen, L. M. Veca and S.-Y. Xie, *J. Am. Chem. Soc.*, 2006, **128**, 7756–7757.
37 L. Zheng, Y. Chi, Y. Dong, J. Lin and B. Wang, *J. Am. Chem. Soc.*, 2009, **131**, 4564–4565.
38 H. Li, X. He, Z. Kang, H. Huang, Y. Liu, J. Liu, S. Lian, C. H. A. Tsang, X. Yang and S. T. Lee, *Angew. Chem., Int. Ed.*, 2010, **49**, 4430–4434.
39 J. Zhou, C. Booker, R. Li, X. Zhou, T.-K. Sham, X. Sun and Z. Ding, *J. Am. Chem. Soc.*, 2007, **129**, 744–745.
40 H. Liu, T. Ye and C. Mao, *Angew. Chem., Int. Ed.*, 2007, **46**, 6473–6475.
41 S. C. Ray, A. Saha, N. R. Jana and R. Sarkar, *J. Phys. Chem. C*, 2009, **113**, 18546–18551.
42 S.-T. Yang, X. Wang, H. Wang, F. Lu, P. G. Luo, L. Cao, M. J. Meziani, J.-H. Liu, Y. Liu, M. Chen, Y. Huang and Y.-P. Sun, *J. Phys. Chem. C*, 2009, **113**, 18110–18114.
43 Y. Dong, N. Zhou, X. Lin, J. Lin, Y. Chi and G. Chen, *Chem. Mater.*, 2010, **22**, 5895–5899.
44 L. Cao, X. Wang, M. J. Meziani, F. Lu, H. Wang, P. G. Luo, Y. Lin, B. A. Harruff, L. M. Veca, D. Murray, S.-Y. Xie and Y.-P. Sun, *J. Am. Chem. Soc.*, 2007, **129**, 11318–11319.
45 S. T. Yang, L. Cao, P. G. Luo, F. Lu, X. Wang, H. Wang, M. J. Meziani, Y. Liu, G. Qi and Y. P. Sun, *J. Am. Chem. Soc.*, 2009, **131**, 11308–11309.
46 J. Shen, Y. Zhu, X. Yang and C. Li, *Chem. Commun.*, 2012, **48**, 3686–3699.
47 R. Liu, D. Wu, X. Feng and K. Muellen, *J. Am. Chem. Soc.*, 2011, **133**, 15221–15223.
48 Z. Zhang, J. Zhang, N. Chen and L. Qu, *Energy Environ. Sci.*, 2012, **5**, 8869–8890.
49 J. Shen, Y. Zhu, X. Yang, J. Zong, J. Zhang and C. Li, *New J. Chem.*, 2012, **36**, 97–101.
50 L. A. Ponomarenko, F. Schedin, M. I. Katsnelson, R. Yang, E. W. Hill, K. S. Novoselov and A. K. Geim, *Science*, 2008, **320**, 356–358.
51 J. Shen, Y. Zhu, C. Chen, X. Yang and C. Li, *Chem. Commun.*, 2011, **47**, 2580–2582.
52 J. Peng, W. Gao, B. K. Gupta, Z. Liu, R. Romero-Aburto, L. Ge, L. Song, L. B. Alemany, X. Zhan, G. Gao, S. A. Vithayathil, B. A. Kaipparettu, A. A. Marti, T. Hayashi, J.-J. Zhu and P. M. Ajayan, *Nano Lett.*, 2012, **12**, 844–849.
53 Y. Li, Y. Hu, Y. Zhao, G. Shi, L. Deng, Y. Hou and L. Qu, *Adv. Mater.*, 2011, **23**, 776–780.
54 M. Zhang, L. Bai, W. Shang, W. Xie, H. Ma, Y. Fu, D. Fang, H. Sun, L. Fan, M. Han, C. Liu and S. Yang, *J. Mater. Chem.*, 2012, **22**, 7461–7467.
55 Y. Dong, J. Shao, C. Chen, H. Li, R. Wang, Y. Chi, X. Lin and G. Chen, *Carbon*, 2012, **50**, 4738–4743.
56 J. Lu, P. S. E. Yeo, C. K. Gan, P. Wu and K. P. Loh, *Nat. Nanotechnol.*, 2011, **6**, 247–252.
57 K. P. Loh, Q. Bao, G. Eda and M. Chhowalla, *Nat. Chem.*, 2010, **2**, 1015–1024.
58 H. Tetsuka, R. Asahi, A. Nagoya, K. Okamoto, I. Tajima, R. Ohta and A. Okamoto, *Adv. Mater.*, 2012, **24**, 5333–5338.
59 Z. Li, W. Zhang, Y. Luo, J. Yang and J. G. Hou, *J. Am. Chem. Soc.*, 2009, **131**, 6320–6321.
60 D. B. Shinde and V. K. Pillai, *Chem.–Eur. J.*, 2012, **18**, 12522–12528.
61 L. Lin and S. Zhang, *Chem. Commun.*, 2012, **48**, 10177–10179.
62 D. Pan, L. Guo, J. Zhang, C. Xi, Q. Xue, H. Huang, J. Li, Z. Zhang, W. Yu, Z. Chen, Z. Li and M. Wu, *J. Mater. Chem.*, 2012, **22**.

63 Y. Zhu, S. Murali, M. D. Stoller, A. Velamakanni, R. D. Piner and R. S. Ruoff, *Carbon*, 2010, **48**, 2118–2122.
64 W. Chen, L. Yana and P. R. Bangalb, *Carbon*, 2010, **48**, 1146–1152.
65 S. Chen, J.-W. Liu, M. L. Chen, X. W. Chen and J. H. Wang, *Chem. Commun.*, 2012, **48**, 7637–7639.
66 H. Liu, X. Zhang, X. Wu, L. Jiang, C. Burda and J.-J. Zhu, *Chem. Commun.*, 2011, **47**, 4237–4239.
67 H. Li, X. He, Y. Liu, H. Huang, S. Lian, S. T. Lee and Z. Kang, *Carbon*, 2011, **49**, 605–609.
68 Y. Li, Y. Zhao, H. Cheng, Y. Hu, G. Shi, L. Dai and L. Qu, *J. Am. Chem. Soc.*, 2011, **134**, 15–18.
69 F. Yang, M. Zhao, B. Zheng, D. Xiao, L. Wu and Y. Guo, *J. Mater. Chem.*, 2012, **22**, 25471–25479.
70 K. Ikehata and M. G. El-Din, *J. Environ. Eng. Sci.*, 2006, **5**, 81–135.
71 T. Gokus, R. R. Nair, A. Bonetti, M. Böhmler, A. Lombardo, K. S. Novoselov, A. K. Geim, A. C. Ferrari and A. Hartschuh, *ACS Nano*, 2009, **3**, 3963–3968.
72 K. Sung-Soo, C. Jeong-Yong, K. Kwan and S. Byeong-Hyeok, *Nanotechnology*, 2012, **23**, 125301.
73 X. Yan, B. Li, X. Cui, Q. Wei, K. Tajima and L. S. Li, *J. Phys. Chem. Lett.*, 2011, **2**, 1119–1124.
74 C. Hu, Y. Liu, Y. Yang, J. Cui, Z. Huang, Y. Wang, L. Yang, H. Wang, Y. Xiao and J. Rong, *J. Mater. Chem. B*, 2013, **1**, 39–42.
75 Z. Luo, Y. Lu, L. A. Somers and A. T. C. Johnson, *J. Am. Chem. Soc.*, 2009, **131**, 898–899.
76 D. Li, M. B. Muller, S. Gilje, R. B. Kaner and G. G. Wallace, *Nat. Nanotechnol.*, 2008, **3**, 101–105.
77 L. Zhang, Y. Xing, N. He, Y. Zhang, Z. Lu, J. Zhang and Z. Zhang, *J. Nanosci. Nanotechnol.*, 2012, **12**, 2924–2928.
78 S. Kim, S. W. Hwang, M.-K. Kim, D. Y. Shin, D. H. Shin, C. O. Kim, S. B. Yang, J. H. Park, E. Hwang, S. H. Choi, G. Ko, S. Sim, C. Sone, H. J. Choi, S. Bae and B. H. Hong, *ACS Nano*, 2012, **6**, 8203–8208.
79 A. P. Alivisatos, *Science*, 1996, **271**, 933–937.
80 D. Pan, J. Zhang, Z. Li, C. Wu, X. Yan and M. Wu, *Chem. Commun.*, 2010, **46**, 3681–3683.
81 H. Li, X. He, Y. Liu, H. Huang, S. Lian, S. T. Lee and Z. Kang, *Carbon*, 2011, **49**, 605–609.
82 J. Lu, J. X. Yang, J. Z. Wang, A. L. Lim, S. Wang and K. P. Loh, *ACS Nano*, 2009, **3**, 2367–2375.
83 H. X. Zhao, L. Q. Liu, Z. D. Liu, Y. Wang, X. J. Zhao and C. Z. Huang, *Chem. Commun.*, 2011, **47**, 2604–2606.
84 Z. A. Qiao, Y. Wang, Y. Gao, H. Li, T. Dai, Y. Liu and Q. Huo, *Chem. Commun.*, 2010, **46**, 8812–8814.
85 S. Zhu, J. Zhang, X. Liu, B. Li, X. Wang, S. Tang, Q. Meng, Y. Li, C. Shi, R. Hu and B. Yang, *RSC Adv.*, 2012, **2**, 2717–2720.
86 W. D. Sheng, M. Korkusinski, A. Güçlü, M. Zielinski, P. Potasz, E. Kadantsev, O. Voznyy and P. Hawrylak, *Front. Phys.*, 2012, **7**, 328–352.
87 K. A. Ritter and J. W. Lyding, *Nat. Mater.*, 2009, **8**, 235–242.
88 L. R. Radovic and B. Bockrath, *J. Am. Chem. Soc.*, 2005, **127**, 5917–5927.
89 L. Bao, Z. L. Zhang, Z.-Q. Tian, L. Zhang, C. Liu, Y. Lin, B. Qi and D.-W. Pang, *Adv. Mater.*, 2011, **23**, 5801–5806.
90 W. C. W. Chan and S. M. Nie, *Science*, 1998, **281**, 2016–2018.
91 X. Michalet, F. F. Pinaud, L. A. Bentolila, J. M. Tsay, S. Doose, J. J. Li, G. Sundaresan, A. M. Wu, S. S. Gambhir and S. Weiss, *Science*, 2005, **307**, 538–544.
92 A. M. Smith and S. Nie, *Acc. Chem. Res.*, 2010, **43**, 190–200.
93 R. C. Somers, M. G. Bawendi and D. G. Nocera, *Chem. Soc. Rev.*, 2007, **36**, 579–591.
94 R. Freeman and I. Willner, *Chem. Soc. Rev.*, 2012, **41**, 4067–4085.
95 R. E. Bailey and S. M. Nie, *J. Am. Chem. Soc.*, 2003, **125**, 7100–7106.
96 L. Fan, Y. Hu, X. Wang, L. Zhang, F. Li, D. Han, Z. Li, Q. Zhang, Z. Wang and L. Niu, *Talanta*, 2012, **101**, 192–197.
97 M. L. Mueller, X. Yan, J. A. McGuire and L. S. Li, *Nano Lett.*, 2010, **10**, 2679–2682.
98 L. Tian, D. Ghosh, W. Chen, S. Pradhan, X. Chang and S. Chen, *Chem. Mater.*, 2009, **21**, 2803–2809.
99 C. Frigerio, D. S. M. Ribeiro, S. S. M. Rodrigues, V. L. R. G. Abreu, J. A. C. Barbosa, J. A. V. Prior, K. L. Marques and J. L. M. Santos, *Anal. Chim. Acta*, 2012, **735**, 9–22.
100 Z. Ding, B. M. Quinn, S. K. Haram, L. E. Pell, B. A. Korgel and A. J. Bard, *Science*, 2002, **296**, 1293–1297.
101 N. Myung, Z. Ding and A. J. Bard, *Nano Lett.*, 2002, **2**, 1315–1319.
102 Y. Bae, N. Myung and A. J. Bard, *Nano Lett.*, 2004, **4**, 1153–1161.
103 H. Zhu, X. Wang, Y. Li, Z. Wang, F. Yang and X. Yang, *Chem. Commun.*, 2009, 5118–5120.
104 Z. Qian, J. Zhou, J. Chen, C. Wang, C. Chen and H. Feng, *J. Mater. Chem.*, 2011, **21**, 17635–17637.
105 M. Li, W. Wu, W. Ren, H. M. Cheng, N. Tang, W. Zhong and Y. Du, *Appl. Phys. Lett.*, 2012, **101**, 103107.
106 K. Gong, F. Du, Z. Xia, M. Durstock and L. Dai, *Science*, 2009, **323**, 760–764.
107 K. Parvez, S. Yang, Y. Hernandez, A. Winter, A. Turchanin, X. Feng and K. Müllen, *ACS Nano*, 2012, **6**, 9541–9550.
108 H. Cheng, Y. Zhao, Y. Fan, X. Xie, L. Qu and G. Shi, *ACS Nano*, 2012, **6**, 2237–2244.
109 Y. Ding, H. Cheng, C. Zhou, Y. Fan, J. Zhu, H. Shao and L. Qu, *Nanotechnology*, 2012, **23**, 255605.
110 I. P. Hamilton, B. Li, X. Yan and L. S. Li, *Nano Lett.*, 2011, **11**, 1524–1529.
111 X. Yan, Q. Li and L. S. Li, *J. Am. Chem. Soc.*, 2012, **134**, 16095–16098.
112 D. I. Son, B. W. Kwon, D. H. Park, W. S. Seo, Y. Yi, B. Angadi, C.-L. Lee and W. K. Choi, *Nat. Nanotechnol.*, 2012, **7**, 465–471.
113 Y. Jing, Y. Zhu, X. Yang, J. Shen and C. Li, *Langmuir*, 2010, **27**, 1175–1180.
114 Z. Liu, J. T. Robinson, X. Sun and H. Dai, *J. Am. Chem. Soc.*, 2008, **130**, 10876–10877.
115 X. Sun, Z. Liu, K. Welsher, J. T. Robinson, A. Goodwin, S. Zaric and H. Dai, *Nano Res.*, 2008, **1**, 203–212.
116 D. Wang, L. Wang, X. Dong, Z. Shi and J. Jin, *Carbon*, 2012, **50**, 2147–2154.

117 J. Zhao, G. Chen, L. Zhu and G. Li, *Electrochem. Commun.*, 2011, **13**, 31–33.
118 J. Qiu, S. Zhang and H. Zhao, *Sens. Actuators, B*, 2011, **160**, 875–890.
119 K. Woan, G. Pyrgiotakis and W. Sigmund, *Adv. Mater.*, 2009, **21**, 2233–2239.
120 Z. Yin, S. Sun, T. Salim, S. Wu, X. Huang, Q. He, Y. M. Lam and H. Zhang, *ACS Nano*, 2010, **4**, 5263–5268.
121 C. W. Tang, *Appl. Phys. Lett.*, 1986, **48**, 183.
122 G. Li, V. Shrotriya, J. Huang, Y. Yao, T. Moriarty, K. Emery and Y. Yang, *Nat. Mater.*, 2005, **4**, 864–868.
123 J. Peet, J. Y. Kim, N. E. Coates, W. L. Ma, D. Moses, A. J. Heeger and G. C. Bazan, *Nat. Mater.*, 2007, **6**, 497–500.
124 H. Wang, D. He, Y. Wang, Z. Liu, H. Wu and J. Wang, *Phys. Status Solidi A*, 2011, **208**, 2339–2343.
125 Z. Liu, Q. Liu, Y. Huang, Y. Ma, S. Yin, X. Zhang, W. Sun and Y. Chen, *Adv. Mater.*, 2008, **20**, 3924–3930.
126 Y. Wang, X. Chen, Y. Zhong, F. Zhu and K. P. Loh, *Appl. Phys. Lett.*, 2009, **95**, 063302.
127 Y.-Y. Choi, S. J. Kang, H. K. Kim, W. M. Choi and S. I. Na, *Sol. Energy Mater. Sol. Cells*, 2012, **96**, 281–285.
128 M. Dutta, S. Sarkar, T. Ghosh and D. Basak, *J. Phys. Chem. C*, 2012, **116**, 20127–20131.
129 S. S. Kim, J. H. Yum and Y. E. Sung, *J. Photochem. Photobiol., A*, 2005, **171**, 269–273.
130 Z. Lu, J. Xu, X. Xie, H. Wang, C. Wang, S.-Y. Kwok, T. Wong, H. L. Kwong, I. Bello, C.-S. Lee, S.-T. Lee and W. Zhang, *J. Phys. Chem. C*, 2011, **116**, 2656–2661.
131 A. K. K. Kyaw, X. W. Sun, J. L. Zhao, J. X. Wang, D. W. Zhao, X. F. Wei, X. W. Liu, H. V. Demir and T. Wu, *J. Phys. D: Appl. Phys.*, 2011, **44**, 045102.